

การเตรียมเม็ดเหล็กบนตัวกลางที่เป็นวัตถุแข็ง



นาย เศรษฐ์วัฒน์ ห่อมณี

สถาบันวิทยบริการ

จุฬาลงกรณ์มหาวิทยาลัย

วิทยานิพนธ์นี้เป็นส่วนหนึ่งของการศึกษาตามหลักสูตรปริญญาวิทยาศาสตรมหาบัณฑิต

สาขาวิชาการจัดการสิ่งแวดล้อม (สหสาขาวิชา)

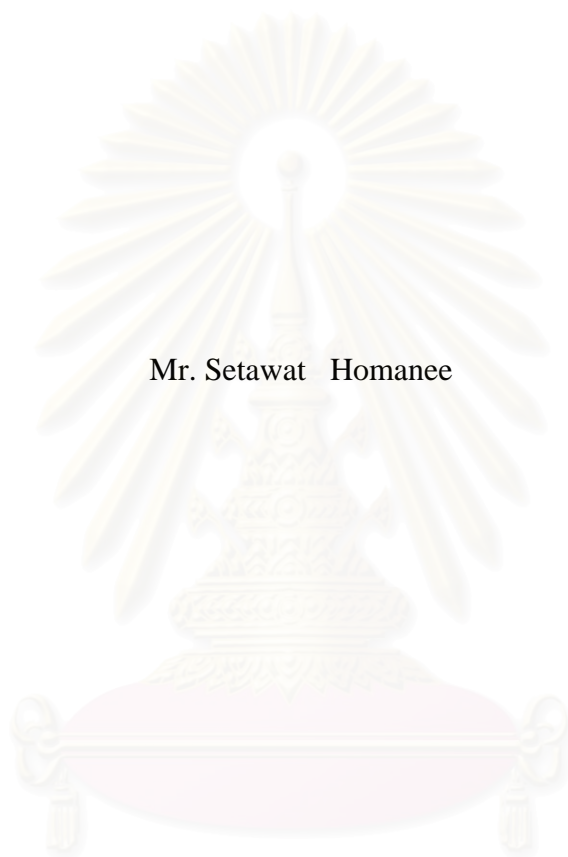
บัณฑิตวิทยาลัย จุฬาลงกรณ์มหาวิทยาลัย

ปีการศึกษา 2548

ISBN 974-53-2620-8

ลิขสิทธิ์ของจุฬาลงกรณ์มหาวิทยาลัย

IRON PELLETTIZATION WITH VARIOUS SEEDING MATERIALS



Mr. Setawat Homanee

A Thesis Submitted in Partial Fulfillment of the Requirements
for the Degree of Master of Science Program in Environmental Management
(Inter-Department)

Graduate School

Chulalongkorn University

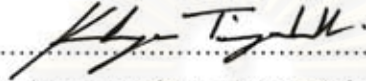
Academic Year 2005

ISBN 974-53-2620-8

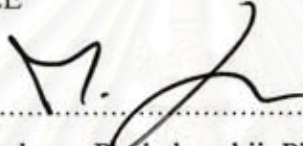
Copyright of Chulalongkorn University


Thesis Title Iron Pelletization with Various Seeding Materials
By Mr. Setawat Homanee
Filed of study Environmental Management
Thesis Advisor Associate Professor Jin Anotai, Ph.D.
Thesis Co-advisor Professor Chih Hsiang Liao, Ph.D.

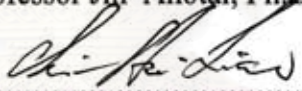
Accepted by the Graduate School, Chulalongkorn University in Partial
Fulfillment of the Requirements for the Master 's Degree

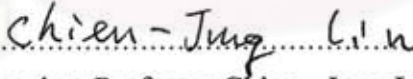

..... Dean of the Graduate School
(Assistant Professor M.R. Kalaya Tingsabdh, Ph.D.)

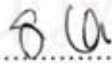
THESIS COMMITTEE


..... Chairman
(Manaskorn Rachakornkij, Ph.D.)


..... Thesis Advisor
(Associate Professor Jin Anotai, Ph.D.)


..... Thesis Co-advisor
(Professor Chih - Hsiang Liao, Ph.D.)


..... Member
(Associate Professor Chien - Jung Lin, Ph.D.)


..... Member
(Assistant Professor Sutha Khaodhiar, Ph.D.)

เศรษฐวัฒน์ ห่อมณี: การเตรียมเม็ดเหล็กบนตัวกลางที่เป็นวัสดุแข็ง. (IRON PELLETTIZATION WITH VARIOUS SEEDING MATERIAL) อ. ที่ปรึกษา: รศ. ดร. จินต์ อโณทัย , อ.ที่ปรึกษาร่วม: Prof. Chih-Hsiang Liao, Ph.D. 97 หน้า. ISBN 974-53-2620-8.

ในช่วงหลายปีที่ผ่านมา กระบวนการเหล็กประจุศูนย์ถูกใช้อย่างกว้างขวางในการบำบัดน้ำเสีย ด้วยวิธีทางเคมี เช่น ใช้ในการกำจัดไนเตรท เพราะกระบวนการนี้มีประสิทธิภาพสูงแต่ต้นทุนต่ำ และแม้ว่าจะมีเหล็กปริมาณมากเกิดขึ้นจากกระบวนการนี้ แต่ของเสียเหล่านี้ไม่เป็นอันตรายต่อสิ่งแวดล้อม ดังนั้นเพื่อกำจัดปัญหาที่เกิดขึ้น จึงมีการศึกษาการนำเอาเหล็กที่เกิดขึ้นจากกระบวนการเหล็กประจุศูนย์กลับมาใช้ใหม่โดยการทำให้เหล็กให้อยู่ในรูปเหล็กออกไซด์ แล้วนำไปเคลือบบนผิวของทรายในถังปฏิกรณ์แบบฟลูอิดไดซ์เบด ซึ่งสามารถช่วยลดปริมาณความชื้นที่มีในของเสียเมื่อเปรียบเทียบกับกระบวนการบำบัดแบบทั่วไป ในการศึกษานี้จะใช้วัสดุตัวกลางหลายชนิด เพื่อเปรียบเทียบประสิทธิภาพในการกำจัดเหล็กเฟอร์รัสออก จากนี้ระบบการเติมอากาศและกระบวนการบำบัดแบบเฟนตัน เพื่อเปรียบเทียบประสิทธิภาพในการเปลี่ยนเฟอร์รัสไอออนให้เป็นเฟอร์ริกไอออน ผลจากการศึกษากระบวนการเฟนตันที่เคลือบเหล็กบนทราย แสดงให้เห็นว่า ปริมาณเหล็กจะเคลือบติดอยู่ที่ผิวของทรายได้มากที่สุดที่พีเอช 6.5 อีกทั้งระบบการหมุนเวียนน้ำยังสามารถส่งผลให้เกิดการตกตะกอนของเหล็กโดยจะมีผลมากที่สุดที่อัตราการไหล 2,100 มิลลิลิตรต่อนาที (การขยายตัวของชั้นตัวกลางเท่ากับ 0.5) ปริมาณทราย 400 กรัมต่อลิตร สามารถกำจัดเหล็กได้ถึง 98 เปอร์เซ็นต์ จากปริมาณเหล็กทั้งหมด 185 มิลลิกรัมต่อลิตร ภายในเวลา 2 ชั่วโมง ซึ่งค่าความจุในการเคลือบเท่ากับ 0.456 มิลลิกรัมต่อกรัม ความสามารถในการเคลือบเหล็กบนผิวทรายจะลดลงเมื่อมีการนำตัวกลางที่เคลือบนั้นกลับมาใช้ใหม่และมีปริมาณเหล็กสะสมบนผิวทราย 3.56 มิลลิกรัมต่อกรัมของทราย ในรอบที่ 11 ขณะที่กระบวนการฟลูอิดไดซ์เบดแบบสามเฟสต้องใช้อัตราการไหล 20 มิลลิลิตรต่อนาที โดยค่าความจุในการเคลือบจะเท่ากับ 0.431 และ 0.417 มิลลิกรัมต่อกรัม ในการเคลือบบนผิวทรายและอะลูมินาออกไซด์ตามลำดับ ผลการศึกษาแสดงให้เห็นว่าเม็ดเหล็กที่ได้จากการเตรียมด้วยกระบวนการฟลูอิดไดซ์แบบสามเฟสจะเสถียรกว่า และนำไปใช้ในวงพีเอชที่กว้างกว่า สำหรับการศึกษาศามารถในการดูดซับเพื่อกำจัดทองแดงด้วยเม็ดเหล็กที่เตรียมขึ้นมา สามารถอธิบายได้ด้วยสมการของแลงมัวร์ ไอโซเทอม ซึ่งค่าความจุในการดูดซับสูงสุดของกระบวนการเคลือบบนทรายด้วย ฟลูอิดไดซ์, กระบวนการเคลือบบนทรายด้วยฟลูอิดไดซ์แบบสามเฟส, และการเคลือบบนอะลูมินาด้วย ฟลูอิดไดซ์แบบสามเฟส มีค่าเท่ากับ 0.249, 0.3, และ 0.222 มิลลิกรัมทองแดงต่อกรัมของเม็ดเหล็ก ตามลำดับ

สาขาวิชาการจัดการสิ่งแวดล้อม(สหสาขาวิชา)
ปีการศึกษา 2548

ลายมือชื่อนิติ..... *เศรษฐวัฒน์ ห่อมณี*
ลายมือชื่ออาจารย์ที่ปรึกษา..... *[Signature]*
ลายมือชื่ออาจารย์ที่ปรึกษาร่วม..... *Chih-Hsiang Liao*

4789491020: MAJOR ENVIRONMENTAL MANAGEMENT

KEY WORD: FERROUS/ FERRIC/ IRON PRECIPITATION/ FLUIDIZED BED/ COPPER

SETAWAT HOMANEE: IRON PELLETTIZATION WITH VARIOUS SEEDING
MATERAILS. THESIS ADVISOR: ASSOC. PROF. JIN ANOTAI, Ph.D.
THISIS CO-ADVISOR: PROF. CHIH-HSIANG LIAO, Ph.D. 97 pp.
ISBN 974-53-2620-8.

Recently, zero valent metals process was widely used for chemical treatments such as nitrate removal because this process is higher efficiency at low cost and leads to non-toxic waste. Nevertheless, the large amounts of iron were produced from zero valent metal process. This research approached this problem by coating iron oxide onto the surface of quartz sand in a fluidized bed reactor which could reduce sludge volume significantly due to denser property of the pellet compared to puffy sludge. This study attempts to utilize several seeding materials as the media in the fluidized bed process for ferrous removal. Additionally, Aeration and fenton pretreated were varied for changing ferrous to ferric ion was concentrated for process comparison. The result from fenton pretreated iron coated sand (F-ICS) showed that higher amount of iron tends to attach on the sand surface at pH 6.5. The recirculation rate was also found to affect iron precipitation in fluidize bed and the optimum flow rate was 2,100 mL/min (0.5 bed expand). Sand of 400 g/L was found to be sufficient to remove 98% of 185 mg/L of total iron within 2 hr which provide specific coating capacity 0.456 mg/g. Iron coating ability of F-ICS seems to be diminished when reused repeatedly with the iron accumulation of 3.56 mg/g sand at the 11th cycle. While, three phase fluidized bed process was achieved at 20 mL/min which produce coating capacity 0.431 and 0.417 mg/g for quartz sand (T-ICS) and aluminum oxide (T-ICAO) respectively. The results indicated the iron pellets obtained from three phase fluidized bed process have more stable at wider pH range. The adsorbed ability of iron pellets for the removal of copper were explained by Langmuir adsorption isotherm which provide a maximum adsorption capacities 0.249, 0.300 and 0.222 mg Cu/g for F-ICS, T-ICS and T-ICAO respectively. SEM and EDX spectrum reported that percent of iron occurred following iron pelletization process and copper became one of the principle elements on the surface of iron pellets after adsorption process.



Field of study: Environmental management
(Inter-Department)
Academic year 2005

Student's signature... *Setawat Homanee*
Advisor's signature... *Jin Anotai*
Co-advisor's signature... *Chih-Hsiang Liao*

ACKNOWLEDGEMENTS

Firstly, I would like to express sincere thanks to my mother, father and my family for their encouragement. I do wish to express my grateful appreciation and gratitude to Dr. Jin Anotai, Dr. Chih-Hsiang Liao and Dr. Chien-Jung Lin for the good opportunity that I conducted a research in Taiwan. I would like to express thanks to Chalermchai Raungchainikom, Ph.D student from NRC-EHWM, Chulalongkorn University who was the most helpful in providing useful information. Furthermore, I express my grateful appreciation to Hsing-Chen Lu, Ph.D students and every students in Prof. Juu En Chang's laboratory, Departments of Environmental Engineering,, National Chen-Kung University, Tainan, Taiwan who were supported instruments for data analysis.

Besides, I would like to express my sincere appreciation and gratitude my friends in NRC-EHWM, KMUTT, CNU, NCKU, Dr. Manaskorn Rachakornkij,, Chairman of the committee, and all committees for their encouragements and constructive suggestion throughout this work. Furthermore, I would like to thank all staffs at laboratory in Department of Environmental Engineering, King's Mungkut University of Technology Thonbury.

The research was sponsored by the Taiwan National Science Council (NSC) under project No.: NSC 93-2211-E-041-001 and International Postgraduate Programs in Environmental and Hazardous waste Management, National Research Center for Environmental and Hazardous Waste Management (NRC-EHWM), Chulalongkorn University.

TABLE OF CONTENTS

	Page
ABSTRACT (IN THAI).....	iv
ABSTRACT (IN ENGLISH).....	v
ACKNOWLEDGEMENTS.....	vi
TABLE OF CONTENTS.....	vii
LIST OF TABLES.....	xii
LIST OF FIGURES.....	xiii
NOMENCLATURE.....	xvii
CHAPTER	
I INTRODUCTION.....	1
1.1 Zero Valent Process.....	1
1.2 Research Aspect.....	3
1.2.1 Objectives.....	3
1.2.2 Hypotheses.....	3
1.2.3 Scopes of the Study.....	4
1.3 Advantages of Research Studies.....	4

CHAPTER	Page
II BACKGROUND AND LITERATURE REVIEW...	5
2.1 Background.....	5
2.1.1 Properties of Iron.....	5
2.1.2 Oxidation pathway of Ferrous Ion.....	5
2.1.3 Iron Oxide.....	8
2.1.4 Fluidization.....	9
2.1.5 Heavy Metal Adsorption by Iron Oxide.....	11
2.1.5.1 Properties Relevant to Iron Oxide.....	11
2.1.5.2 Specific Adsorption of Heavy Metals.....	15
2.1.6 Sorption Isotherm.....	18
2.2 Literature Reviews.....	19
2.2.1 The Preparation of Iron Pellet.....	19
2.2.2 Heavy Metals Removal by Adsorption Process	21

CHAPTER	Page
IV RESULTS AND DISCUSSION.....	32
4.1 Iron Pellets Preparation.....	32
4.1.1 Iron Coated Sand (ICS).....	32
4.1.1.1 Fenton Pretreatment.....	32
4.1.1.2 Aeration Treatment.....	42
4.1.2 Iron Coated Sand Leaching Tests.....	47
4.1.3 Iron Coated Aluminum Oxide (ICAO).....	49
4.2 Iron Pellets Application for Copper Removal.....	55
4.2.1 Equilibrium Times.....	55
4.2.2 Effect of pH on Copper Removal.....	56
4.2.3 Adsorption Isotherm.....	58
4.2.4 Surface Characterization of Iron pellets After Copper Adsorption.....	61
4.2.5 Managerial Prospect.....	63

CHAPTER	Page
V CONCLUSIONS AND RECOMMENDATIONS....	64
5.1 Conclusions.....	64
5.2 Recommendations.....	65
REFERENCES.....	66
APPENDICES.....	72
Appendix A.....	73
Appendix B.....	80
Appendix C.....	81
Appendix D.....	85
Appendix E.....	88
Appendix F.....	89
BIOGRAPHY.....	97

LIST OF TABLES

Table	Page
2.1 Polymorphs of Fe oxide.....	8
2.2 Cation adsorption studies on Fe oxides.....	15
2.3 Anion adsorption studies on Fe oxides.....	15
3.1 Seeding materials properties.....	25
4.1 First-order rate constants for iron removal at various ferrous concentrations and sand dosages in fenton pretreated fluidized bed process	38
4.2 Surface composition of sequential batch of F-ICS by SEM-EDS.....	42
4.3 Surface composition of F-ICS and T-ICS by SEM-EDS.....	44
4.4 Comparisons of percent leaching between F-ICS and T-ICS at 72 hrs...	49
4.5 Surface composition of F-ICS and T-ICS by SEM-EDS.....	53
4.6 Summary of the adsorption isotherm by Langmuir and Freundlich isotherm of copper ion on different types of iron pellets.....	61
4.7 Surface composition of F-ICS, T-ICS and T-ICAO after copper adsorption by SEM-EDS.....	63

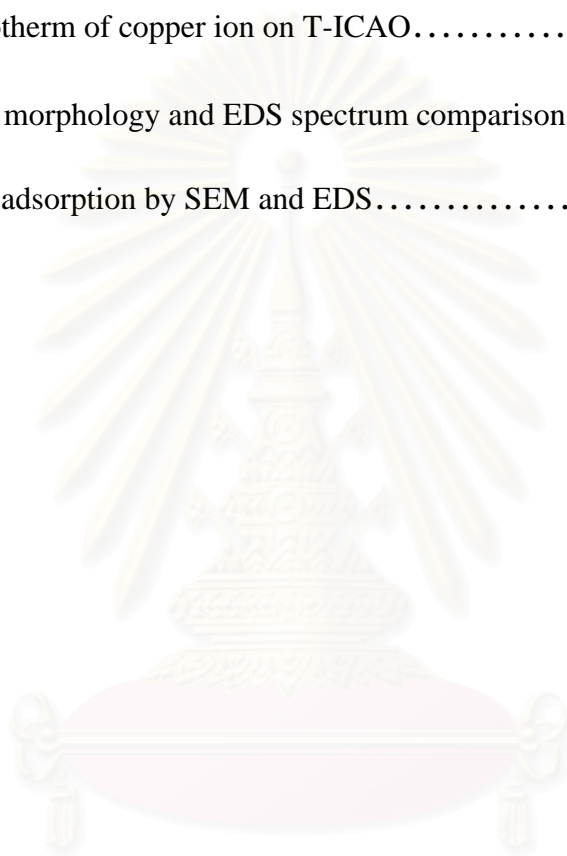
LIST OF FIGURES

Figure	Page
1.1 Schematic of zero valent process for the removal of nitrate.....	1
2.1 The model proposed by Parks and de Bruyn (1962) describing about surface charge and surface potential.....	12
2.2 The reaction of surface groups of Fe-oxide particle with water proceeds in two steps: (Step1) and hydration (step2).....	12
2.3 The effect of pH on the adsorption of various heavy metals by synthetic hematite and goethite.....	16
2.4 The effect of pH and electrolyte concentration on the adsorption of Cu and Pb by synthetic goethite.....	17
2.5 Sorption Isotherms.....	19
3.1 Schematic of fluidized bed reactors for iron pelletization.....	26
3.2 Experimental diagram.....	27
3.3 Fenton pretreated operation procedure for iron coated sand.....	29
3.4 Three phase fluidized bed operation procedure for iron coated sand.....	30
3.5 Fenton pretreated operation procedure for iron coated aluminum oxide...	31

Figure	Page
4.1 Effect of pH on the iron removal in fluidized bed process.....	33
4.2 pC-pH diagram for hydrolysis products of Fe ³⁺	33
4.3 Characteristics of fenton pretreated iron coated sand (F-ICS) by XRD analysis.....	34
4.4 Effect of flow rate on the iron removal in fluidized bed process.....	35
4.5 Effect of sand dosage on the iron removal in fluidized bed reactor.....	36
4.6 Effect of initial iron concentration on the iron removal in fluidized bed process.....	39
4.7 Durability of sand for iron removal efficiency.....	39
4.8 Surface morphology and EDS spectrum of F-ICS by SEM and EDS....	41
4.9 Effect of air flow rate on the iron removal in fluidized bed process.....	43
4.10 Characteristics of three phase iron coated sand (T-ICS) by XRD analysis.	44
4.11 Surface morphology and EDS spectrum comparisons of ICS by SEM and EDS.....	45
4.12 Effect of sand dosage on the iron removal in fluidized bed process.....	46
4.13 F-ICS leaching test as a function of time.....	48
4.14 T-ICS leaching test as a function of time.....	48

Figure	Page
4.15 Effect of pH on the iron removal in fluidized bed process.....	50
4.16 Characteristics of three phase iron coated aluminum oxide (T-ICAO) by XRD analysis.....	51
4.17 Surface morphology and EDS spectrum comparisons of ICS by SEM and EDS.....	52
4.18 Effect of aluminum oxide dosage on the iron removal in fluidized bed process.....	54
4.19 Equilibrium time of fresh sand, F-ICS and Y-ICS for adsorption copper.	55
4.20 The iron leaching from media carrier as a function of time in adsorption process.....	56
4.21 Equilibrium time of fresh Al_2O_3 and T-ICAO for adsorption copper....	57
4.22 Effect of pH on copper removal by F-ICS.....	57
4.23 Effect of pH on copper removal by T-ICS.....	58

Figure		Page
4.24	The isotherm of copper ion on F-ICS.....	60
4.25	The isotherm of copper ion on T-ICS.....	60
4.26	The isotherm of copper ion on T-ICAO.....	60
4.27	Surface morphology and EDS spectrum comparisons of iron pellets after copper adsorption by SEM and EDS.....	62



สถาบันวิทยบริการ
จุฬาลงกรณ์มหาวิทยาลัย

NOMENCLATURE

C	=	liquid phase chemical concentration (M/L ³)
C_{ads}	=	concentration in solid phase (M/L)
C_{aq}	=	concentration in aqueous phase (M/L)
C_e	=	equilibrium concentration (M/L)
q	=	mass of chemical sorbed normalized by mass of resin (M/M)
K_d	=	linear isotherm coefficient (L ³ /M)
K_F	=	Freundlich isotherm coefficient (L ³ /M)
K_L	=	Langmuir isotherm coefficient (L ³ /M)
A_M	=	maximum adsorption capacity (M/M)

สถาบันวิทยบริการ
จุฬาลงกรณ์มหาวิทยาลัย

CHAPTER I

INTRODUCTION

1.1 Zero-Valent Iron Process

Recently, zero-valent iron (Fe^0) served as an in-situ and ex-situ groundwater treatment reductant is highly interested for removing chlorinated compounds, heavy metals, and inorganics such as nitrate (Kim and Carraway, 2000; Cheng and Wu, 2000; Alowitz and Scherer, 2002; Liao et. al., 2003). Figure 1.1 showed that the example of Fe^0 process for the removal of nitrate, Fe^0 is oxidized to ferrous ion (Fe^{2+}) and two electrons are released and captured by nitrate which is an oxidant presence in solution. This Fe^0 process is very reactive in the acidic range which promotes the corrosion of metallic iron. Acidic condition created by CO_2 bubbling is selected for this study since it can avoid any introduction of alien species such as SO_4^{2-} , Cl^- , NO_3^- and CH_3COO^- from H_2SO_4 , HCl , HNO_3 and CH_3COOH addition, respectively, into the treated effluent (Hsu et al., 2004).

According to Fe^0/CO_2 process, a great amount of Fe^{2+} generated from Fe^0 as the major product is of concern to groundwater quality. Normally, the conventional process that was used to remove Fe^{2+} is a chemical precipitation.

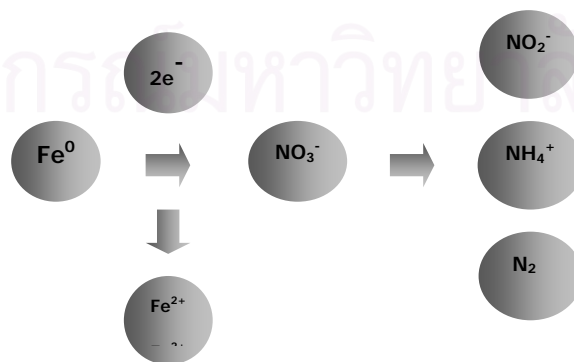


Figure 1.1 Schematic of Fe^0 process for the removal of nitrate

Soluble Fe^{2+} was transformed to solid species such as iron oxide or hydroxide compounds and settles out from the solution. Commonly, suitable pH for iron precipitation is around neutral. However, the settling process is often accelerated by addition of a polymer coagulant, which gathers the insoluble metal compound particles into a coarse floc that can settle rapidly by gravity. Regarding the disadvantage of precipitation process, a large volume of sedimentation tank and a sludge dewatering facility for the removal of sludge moisture content are required. Therefore, the iron precipitation and/or crystallization onto media in a fluidized-bed reactor is of interest as an alternative process. Generally, this method is applied to remove hardness in water softening (Van Der Veen and Graveland, 1988; Chen et al., 2000) and heavy metal (Zhou et al., 1999). To eliminate sludge disposal problem, the application of iron coated media can be further applied in wastewater treatment process such as heavy metal adsorption and Fenton process.

This study attempts to utilize several seeding materials as the media in the fluidized bed process for Fe^{2+} removal. Additionally, various processes for transforming Fe^{2+} to Fe^{3+} was also focused. Several specific experiments were conducted to determine the effect of process parameters including initial pH, bed expansion, media dosages, and initial Fe^{2+} concentration. Quartz sand was used principally as the carrier whereas aluminum oxide was used for media comparison purpose.

Iron pellets obtained from the experiments were further tested for adsorption capability since it is well known that iron oxide is an excellent and regenerable adsorbent for metal adsorption (Lai and Chen, 2000; Lo et al, 1997). Copper was used as a target metal for this matter in a batch operation.

1.2 Research Aspect

The results of this work will provide valuable information on iron coating process and effect of raw granule material which can be further applied in both water and wastewater treatment schemes to eliminate and/or reduce sludge disposal quantity. In addition, the results from copper adsorption study will offer an alternative for reutilizing these iron-coated carriers which will generate more benefits.

1.2.1 Objectives

This study was originally designed to determine the removal of Fe^{2+} ion resulting from the corrosion of metallic iron in the Fe^0/CO_2 process by using iron precipitation and/or crystallization processes in the fluidized bed reactor. By creating densified iron pellet, surface area of settling tank as well as the sludge volume can be minimized. Additionally, obtained iron pellets were further examined for their sorbability of heavy metals. The objectives of this study can be specified as follows:

1. To investigate optimum conditions for iron pellets precipitation and/or crystallization onto media surface.
2. To investigate the effect of media materials on iron pelletization.
3. To determine the capability of iron pellets for heavy metal sorption.

1.2.2 Hypotheses

1. Iron pelletization depends mainly on the operating conditions.
2. Surface properties of seeding material have effects on the interaction between iron oxide and media.
3. Iron oxide possesses the ability to sorb heavy metal and is regenerable.

1.2.3 Scopes of the Study

All experiments were conducted in a batch manner. Two types of seeding materials, i.e., sand (SiO_2) and aluminum oxide (Al_2O_3) were focused although sand was used more intensively. Fenton pretreatment and aeration were used to convert Fe^{2+} to Fe^{3+} prior to precipitate and/or crystallization onto media surface. Obtained iron-coated carriers were examined for their properties, i.e., micro-morphology and surface composition, by SEM and XRD and were tested for their adsorption ability using copper as a target pollutant.

1.3 Advantages of Research Study

This research will create a better alternative to eliminate the Fe^{2+} resulting from iron corrosion. The results from this study provide valuable information on iron pelletization process. The optimum conditions for process operation in both pretreatment cases, i.e. Fenton pretreated and three-phase (aeration) iron pelletizations were revealed. The utilization of iron pellets as an adsorbent were also verified which leads to the reduction of environmental problems as well as disposal cost saving.

Additionally, the use of CO_2 as a pH controlling chemical in Fe^0 process is proposed and proven to be effective. This technique can be further applied in the field.

CHAPTER II

BACKGROUND AND LITERATURE REVIEWS

2.1 Background

2.1.1 Properties of Iron

Iron has atomic number and weight of 26 and 55.85, respectively. It has several stable isotopes including 54 (5.9%), 56 (91.6%), 57 (2.2%) and 58 (0.33%). Its electron configuration is $Ar3d^64s^2$, and its first and second ionization potentials are 7.87V and 16.18V. With its neighbors cobalt ($Z = 27$) and nickel ($Z = 28$), it is one of the "iron triad" of similar metals. Iron is in the center of the periodic table, in the region of "transition metals" where a d-shell of electrons is being filled. The 4s electrons are actually more stable than the 3d electrons, so the d-electrons are actually on the outside of the atom. The d-shell can hold 10 electrons, and as it becomes nearly filled, drops below the 4s electrons in energy. All these atoms filling d-shells make metals that are very much alike; if the d-electrons were more inside, these metals would be even more alike than they are.

2.1.2 Oxidation pathway of Ferrous Ion

Naturally, iron occurs mainly in the forms of Fe^{2+} and Fe^{3+} . A large number of important iron salts are formed with various anions. Fe^{2+} will simultaneously donate an electron in an acidic solution or in the presence of oxygen and being oxidized to Fe^{3+} , so it is a reducing agent. On the other hand, in alkaline solution, Fe^{3+} will possibly accept an electron and reducing itself to Fe^{2+} so it is an oxidizing agent. In acid solution, metallic iron (Fe^0) will reduce H^+ to H_2 , since its electrode potential is -0.44V, well above hydrogen's. As a result, iron is in fact an active element. Most

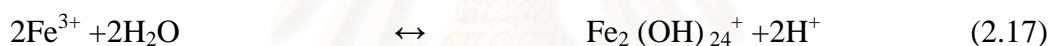
common oxide forms are ferrous oxide (FeO) and ferric oxide (Fe₂O₃). Ferrous oxide is not stable against partial oxidation to Fe²⁺, usually written Fe₃O₄ or FeO·Fe₂O₃. This hard and black substance is called “magnetite”, an important ore of iron and is a very interesting substance in its own right, which will be considered further in connection with magnetism.

When Fe⁰ is added to acidic solution, the pH will increase significantly and rapidly which is attributed to the hydroxyl ion formation during the corrosion of Fe⁰ in the solution according equations (1) and (2) (Ponder et al., 2000).



Fe²⁺ is the Fenton’s reagent apart from H₂O₂ of which when adding together can generate hydroxyl radicals or so called “Fenton process”. The variation of pH may be expected from the related reaction of Fenton reaction in equations (3) to (8) especially, the equation (3) (Pignatello, 1992). The products of Fe²⁺ reacting with oxygen includes magnetite (Fe₃O₄), ferrous hydroxide (Fe(OH)₂), and ferric hydroxide (Fe(OH)₃) according to equations (9) to (12) (Kanel et al., 2005). Furthermore, hydrolysis of Fe³⁺ results in different iron complex species, depending on the redox conditions and pH as described by equations (13) to (17) (Snoeyink and Jenkins, 1980).





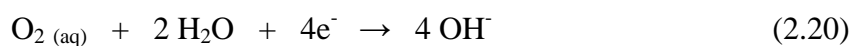
Fe^0 oxidation which involving oxygen to form iron oxide is a very complex process. It is thought to begin with the oxidation of iron to Fe^{2+} .



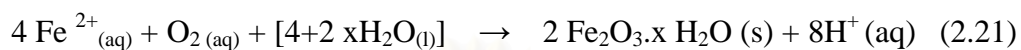
Both water and oxygen are required for the next sequence of reactions. Fe^{2+} are further oxidized to form Fe^{3+} .



The electrons provided from both oxidation steps are used to reduce oxygen as shown:



The Fe^{3+} then combines with oxygen to form ferric oxide which is then hydrated with varying amounts of water. The overall equation for the rust formation may be written as:



2.1.3 Iron Oxide

Iron oxide occurs naturally in several different forms and colors. Indeed, iron is the second most abundant element on earth, representing over 5% of the earth's crust. These natural products tend to be coarse in particle size and contain impurities, making them opaque and dirty. The chemistry of iron is a very complex field where, under different conditions of manufacture, several different polymorphs are produced (Table 2.1).

The oxides are ferrous oxide, FeO and ferric oxide, Fe_2O_3 . Ferrous oxide is not stable against partial oxidation to Fe (II), usually written Fe_3O_4 or $\text{FeO} \cdot \text{Fe}_2\text{O}_3$. This

Table 2.1. Polymorphs of Iron Oxide

Color	Designation	Name	Structure	Crystal System
Yellow	FeOOH	Goethite	Ramsdellite/ hcp oxygen	Orthorhombic
		Akaganeite	Hollandital/ bcc oxygen	Tetragonal
		Lepidochrocite	Boehmite/ ccp oxygen	Orthorhombic
		-	Cdl ₂	Hexagonal
Red	Fe_2O_3	Hermatile Maghemite	Corundum Defect spinel	Hexagonal Cubic
Black	Fe_3O_4	Magnetite	Inverse spinel	Cubic

hard, black substance is *magnetite*, an important ore of iron and a very interesting substance in its own right, which will be considered further in connection with magnetism.

The Fe^{2+} ion is greenish in solution, while the Fe^{3+} is a light violet. The distinct colors of iron compounds are due to the d-electrons, which can interact with light in many interesting ways. Ferrous oxide, as a mineral, is called *hematite* ("blood-stone") and is usually almost black. It leaves a red streak on unglazed porcelain, and in its usually finely-divided condition is a characteristic bright earthy red. In pure form, it is called *rouge*, good for reddening cheeks and polishing glass, or *Venetian red*, a red pigment. The red stains on concrete are ferric oxide, usually from reinforcement rods that are not properly protected from the weather. The red of Mars is ferric oxide, showing that the atmosphere once contained oxygen, the oxygen that is only liberated by life.

2.1.4. Fluidization

Fluidized beds serve many purposes in industry, such as facilitating catalytic and non-catalytic reactions, drying, and other forms of mass transfer. They are especially useful in the precipitation process for example removal a solids particle onto surface of media. Because of introducing fluid up flow through a bed of media, the condition in the bed is almost homogeneous. Moreover, fluidization introduce clear water zone in reactor which can be recharge at the same time with process operation. Therefore, fluidization generates easier technique for precipitate particle onto surface of media.

Importantly, the process must have a good understanding of the factors that affect the behaviors of fluidized beds in order to use them effectively. Therefore, it is crucial to be able to predict how pressure drop will occur under different fluidization conditions. The main concepts to be studied are the minimum fluidization velocity required for the bed of particles and the degree of pressure drop that the upward flowing fluid experiences. By being able to predict these properties, the engineer will be able to design processes for industrial applications and find the best conditions to run the apparatus.

Fluidization involves the passing of fluid upwards through a bed of particles and expanding it. The minimum fluidization velocity is reached when the pressure drop over the column is equal to the weight of the bed divided by its cross-sectional area. (Perry Robert H.) The minimum fluidization velocity tells the engineer what flow of gas is required to expand the bed of particles, and thus how it will behave under a number of flow conditions. Since there are an unlimited number of fluid and particle combinations that can be used in fluidized beds, many mathematical models have been derived for different situations. These equations are based on particle shape, density, and size as well as fluid density, viscosity, etc. The proper equation must be used for each case or else the results will not be accurate. A list of several different models can be found in Fluidization: (Davidson, J. F. et al, 1985). Fluidization is divided up into five regimes: packed (0.01 m/s), particulate (0.038 m/s), bubbling (0.1 m/s), turbulent (1 m/s), fast fluidization (4 m/s), and pneumatic transport (10 m/s). As the fluid velocity supplied to the column is increased, the movement of the bed becomes more active and proceeds through each of these flow patterns.

2.1.5 Heavy Metal Adsorption by Iron Oxide

2.1.5.1 Properties Relevant to Iron Oxide

A. Surface Structure

One of the most important properties of the different Fe oxides is their surface structure and the resultant dependency of surface charge on pH, because the surface is the region of their interaction with solid phases, plants roots, and the soil biota.

In the presence of water, the Fe ions located at the surface of an oxide complete their ligand shell with hydroxyl ions so that the surface becomes completely hydroxylated. For the Fe-O-Fe-bond, the surface reaction may be represented by step 1 (Figure 2.1), resulting in a surface –OH density on hematite of 4.5 to 9 per nm² (Breeuwsma, 1973). The hydroxylation of the surface is then followed by the adsorption of H₂O molecules through H-bonding (step 2), and a monomolecular layer of water is formed (Breeuwsma, 1973).

The amount of adsorbed H₂O in a monomolecular layer increases with the increasing surface area or with a decrease in crystal size (Schulze & Schwertmann, 1984; Schwertmann et al., 1985). It amounts to 0.3 to 0.4 mg m⁻² and appears to be tightly bound (Gast et al., 1974; Breeuwsma, 1973). In goethite, adsorbed H₂O is only completely driven off at about 200 °C.

B. Surface Charge

At the hydroxylated or hydrated surface, positive or negative charge is created by an adsorption or desorption of H⁺ or OH⁻, resulting in a surface potential. Surface charge and surface potential vary with the concentration of H⁺ and OH⁻ ions in solution.

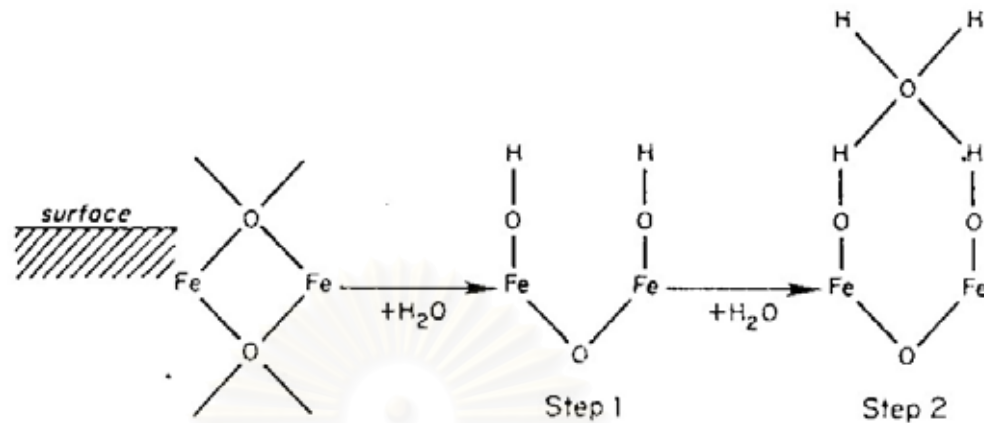


Figure 2.1 The reaction of surface groups of Fe-oxide particle with water proceeds in two steps: (Step1) and hydration (step2)

Therefore, the H⁺ and OH⁻ ions are termed *potential determining ions* (PDI). The model proposed by Parks and de Bruyn (1962) can be presented by Figure 2.2. The pH at which the net variable charge on the surface is zero is called the *point of zero charge* (PZC). From this model it is obvious that the Fe ions do not participate directly in charge development. An excess of positive or negative surface charge is balanced by an equivalent amount of anions (A⁻) or cation (C⁺), respectively, located in the outer part of an electric double layer. In addition to pH, the charge also depends on the concentration of the electrolyte and valence of the ions in the equilibrium

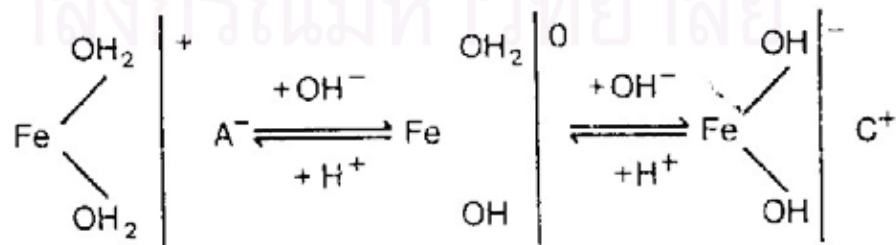


Figure 2.2 The model proposed by Parks and de Bruyn (1962) describe about surface charge and surface potential.

solution, i.e., the ionic strength. Because of its dependency on pH and ionic strength, the charge is called *variable charge*. If the zero net charge is due only to H^+ , OH^- , or metal-hydroxy ions derived from the dissolution of the structural cation, the PZC also is equal to the *isoelectric point* (IEP) (Bowden et al., 1977).

The pH of the PZC of Fe oxides ranges between the various mineral forms (Borggaard, 1983). Specially, adsorbed anions lower the PZC, whereas cations raise the PZC (Parks, 1967). Thus, the PZC of a particular oxide may give different values depending on the kind and extent of foreign ion adsorption. Because natural samples often have anions adsorbed at the surface, their PZC values are generally lower than for their synthetic counterparts (Park, 1965). For example, PZC values of 5.3 to 7.5 were found with natural ferrihydrites because of silicate adsorption (Schwertmann & Fechter, 1982), whereas the value for a pure synthetic sample was around 8. The nearer the PZC is to the natural pH value of the soil, the more susceptible is the polarity of the net charge to small changes in the environmental pH.

Permanent charge arising from isomorphous substitution, as occurs in most layer silicates, contributes little or nothing to the charge of the Fe oxides. An exception is the substitution of Ti^{4+} for Fe^{3+} , which creates positive permanent charge (Tessens & Zauyah, 1982). This may be counterbalanced by substitution of Fe^{2+} for Fe^{3+} as, for example, in titanomaghemite.

C. Ion Adsorption

As mentioned above, surface charge is balanced by adsorption of an equivalent amount of A^- or C^+ , or the respective charged regions of polarizable molecules (counter ions), held in the outer diffuse electric double layer. For electrostatic (coulombic) bonding, where the counter ions are treated as point charges,

the adsorption is termed of nonspecific and depends only on ionic charge. In a multicomponent system, ions of equal charge would be adsorbed according to their activity in solution. The anions Cl^- , NO_3^- , and ClO_4^- and the alkali cations generally behave in this manner. In this particular situation, replacement of one ion by another at constant ionic strength would not change the electrophoretic mobility of the particles. In nonspecific adsorption, a certain degree of specificity may be introduced by ionic size or steric hindrances.

Other anions and cations can, however, be held much more strongly at the oxide surface. This is because the adsorbate penetrates the Fe coordination shell and by ligand exchange becomes covalently bound directly to the structural cation via O and OH groups. This is called *chemisorption*, *specific adsorption*, or *ligand exchange*, and was described by Hingston et al. (1968).

Most ion adsorption studies have been carried out on the two most common minerals, goethite and hematite. Since all the oxides have similar hydroxylated surfaces and acquire pH-dependent charge, however, they could be expected to display similar affinities toward the respective ions.

The amount of a particular ion adsorbed depends mainly on its activity, pH, and the ionic strength of the equilibrium solution. At a given pH, adsorption increases with increasing activity. In many cases this relation may be described by one of the well-known isotherms (e.g., Langmuir, Freundlich, and others). Where adsorption studies have been carried out under different conditions with respect to concentration and nature of the indifferent electrolyte, temperature, pH, or unknown specific surface, etc., the results cannot be validly compared. For this reason only a few samples of adsorption values are given in this discussion. (Tables 2.2 and 2.3)

Specific ion adsorption can occur on a neutral surface, or even on a surface with a charge of the same sign as the ion, and can thus reverse the surface charge, whereas nonspecifically absorbed species cannot. Specific adsorption of polyvalent

Table 2.2 Cations adsorption studies on Fe oxides.

Mineral phase	Cations
Ferrihydrite	Ca; Cu; Eu; Sb; Zn
Goethite	Cd ; Co; Cu Pb; Mn; Hg; Mo; Ni; Zn
Hematite	(NH ₃); Al; Ba; Co; Cu; Eu; Mu; Ni; Ga; Pb; Li; Mg; M; Ag; Zn
Lepidocrocite	U; Mn; Zn
Magnetite/maghemite	Mo ; Co; Zn

Table 2.3 Anion adsorption studies on Fe oxides.

Mineral phase	Anions
Ferrihydrite	Molybdate; borate; sulphate
Goethite	Phosphate; silicate; citrate; Molybdate; selenite; sulphate; CO ₂
Lepidocrocite	Phosphate; silicate
Maghemite/magnetite	Chloride

anions such as HPO_4^{2-} (which has been extensively studied for Fe oxides) may therefore increase the CEC by the creation of additional negative charges; (Wann and Uehara, 1978) suggested that phosphate added to an oxidic soil as a fertilizer also acts as a soil amendment by causing an increase in the adsorption of nutrient cations.

2.1.5.2 Specific Adsorption of Heavy Metals

Heavy metals are adsorbed by goethite and hematite in the order of $\text{Cu} > \text{Pb} > \text{Zn} > \text{Cd} > \text{Co} > \text{Ni} > \text{Mn}$ except for an interchange in position of Cu and Pb for hematite (Grimme, 1968; Hildebrand and Blum, 1974; McKenzie, 1983; Gerth and

Brümmer, 1983). The most important factor determining the extent of adsorption is pH. As pH increases, a steep rise in adsorption occurs within a narrow pH-range (Figures 2.4 and 2.5). The pH range is metal-specific and follows the same order as given above. The pH of maximum increase in adsorption is found to be linearly related to the first hydrolysis constant of the metal $K_1 = (\text{MOH}^+) / (\text{M}^{2+}) \cdot (\text{OH}^-)$. This indicates that the hydrolyzed species (MOH^+) is preferentially adsorbed over the unhydrolyzed one (M^{2+}).

The structure of the surface complex between the functional groups of the Fe oxide and the heavy metal is not fully known. From the measured release of between one and two protons per metal atom adsorbed, several reactions have been proposed (Grimme, 1968; Forbes et al., 1976; McKenzie, 1983) in which mono-(equation (21)) or binuclear (equation (22)) complexes may form:

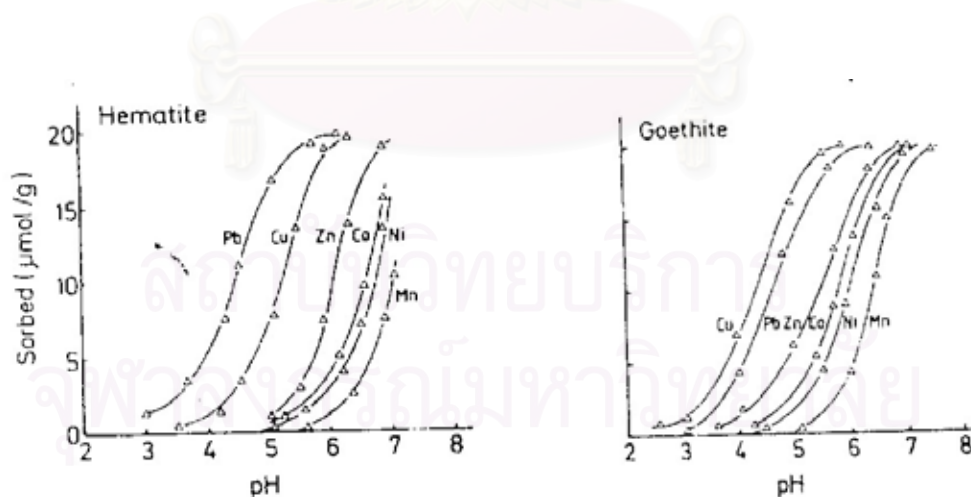


Figure 2.3 The effect of pH on the adsorption of various heavy metals by synthetic hematite and goethite. Heavy metal addition $20 \mu\text{mol g}^{-1}$ Fe oxide (from McKenzie, 1980).

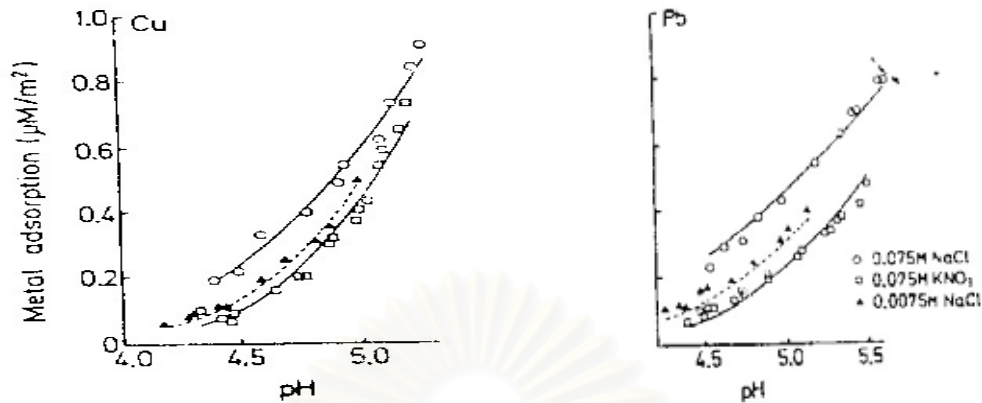
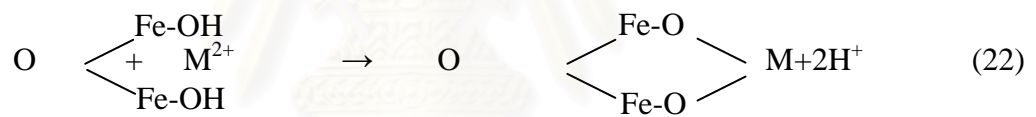
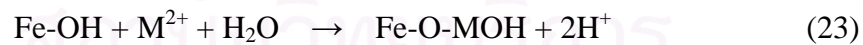


Figure 2.4 The effect of pH and electrolyte concentration on the adsorption of Cu and Pb by synthetic goethite (Barrow et al., 1981). The four-layer model of Bowden et al. (1980), from which the solid lines were calculated, describes the experimental results (dots) very well.



As the pH of the system increases, MOH^+ , the hydroxyl species, rather than M^{2+} will be adsorbed (23).



The strong effect of heavy metal adsorption, which also was found for soils (Gerth & Brümmer, 1983), is of great relevance for the mobility of toxic heavy metals in the soil mantle and thus for groundwater pollution. This is especially so in view of the recently documented acidification of soils in industrial areas. An effect of different anions on heavy metal adsorption also has been noticed and can be preferentially adsorbed over M^{2+} (Barrow et al., 1981).

Time and temperature are two additional factors influencing metal adsorption on iron oxides. Gerth & Brümmer (1983) found a linear relationship between Ni, Zn, and Cd adsorption on goethite and the square root of time, indicating that diffusion processes were involved in this adsorption. Diffusion may be rate-determining when the metals migrate into micropores of the crystal. This process will accelerate with increasing temperature, explaining why adsorption of the above metals increased as the temperature increased from 5 to 35 °C (Gerth & Brümmer, 1983). Migration into micropores also may explain why in some cases significant proportions of the adsorbed heavy metals can be very difficult to re-extract, even with strong acids (Brümmer et al., 1988).

2.1.6 Sorption Isotherm

When the measured adsorption data are plotted against the concentration value of the adsorbate at equilibrium, a graph is obtained called the adsorption isotherm. (Yaron et al., 1996). Three adsorption models are used to describe three different behaviors.

A straight-line relationship implies that the process of adsorption is not affected by solute concentration and that surface of the solid has unlimited capacity for adsorption. Linear adsorption isotherm is appropriate for many species at low solution concentration, but they are not appropriate at higher concentrations when the surface sites for adsorption become filled. (Deutsch, 1997)

Freundlich and Langmuir isotherms are also closely linear at low adsorbate concentration; however, they change slope at higher concentrations. The Freundlich isotherm becomes a curve at higher concentration reflecting lower adsorption at these

values as the adsorption sites become filled. However, there is no total capacity term in the Freundlich isotherm equation, so there is no upper limit on the adsorption.

Linear Sorption Isotherm

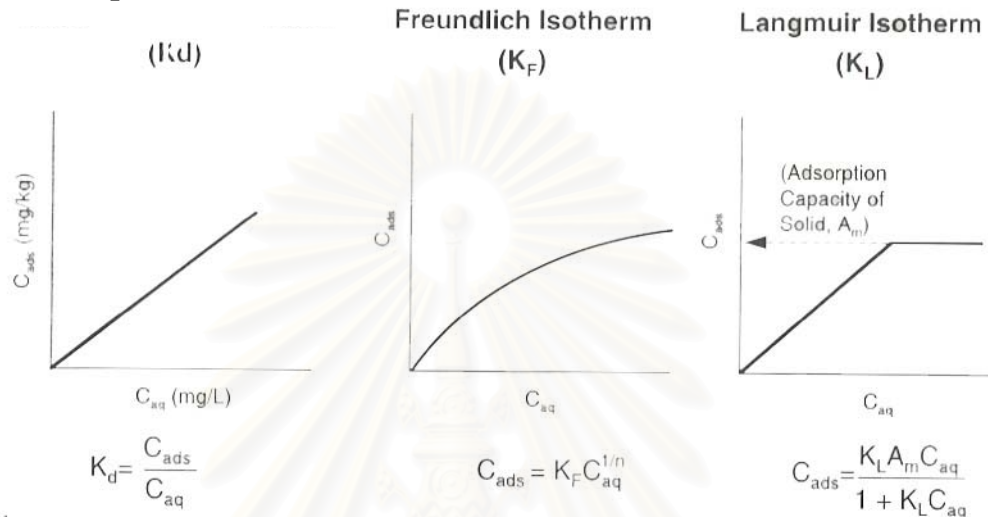


Figure 2.5. Sorption Isotherms

The Langmuir isotherm has a capacity term (A_m) in its definition. Once the concentration of adsorbed species reaches this capacity term, adsorption decrease to zero regardless on any additional increase in adsorbate concentration. (Deutsch, 1997)

2.2 Literature Reviews

2.2.1 Preparation of Iron Pellets

Lo et al. (1997) developed a process for coating iron oxide onto the surface of quartz sand and examined the adsorption property of coated media by using SEM and XRD. Several coating conditions were investigated, e.g., pH, temperature, and iron concentration. Coating pH played very important role in iron oxide formation and heavy metal removal. High pH coating provided more adsorption capacity than at low pH but sacrificing with lower acid resistance property. At higher coating temperature,

the stability of the oxide coatings was enhanced notably. Number of pores and specific surface area of the media increased significantly after iron coating.

Lo and Chen (1997) developed a method for coating hydrated iron-oxide onto the surface of quartz sand. Effect of pH at which iron oxide synthesized and the coating temperature are investigated. Large quantity of iron was coated onto quartz sand in the lower pH range (0.5-2.0) than higher range (8.0-11.0). Moreover, low-pH iron coated sand was more stable in acidic and basic solutions and had better Se (IV) and Se(VI) adsorption properties than those coated at high pH. In kinetic experiments, pseudo-equilibrium of Se (IV) adsorption was attained within 10 min while the Se (VI) required longer time of 1.5 hours.

Xu and Axe (2004) focused on the synthesis and characterization of iron oxide-coated silica. Three-level fractional factorial study was used to determine the optimum conditions for producing goethite-coated silica. Modified adsorption and modified precipitation were used for goethite synthesis and coated with silica. The most significant factor in coating was the particle size of silica. If amount of iron at the surface area of silica increased, particle size of silica decreased. Other factors investigated were coating temperature, initial iron concentration, and contact time which found to be less important. The iron-oxide coatings were non-uniform, concentrated in rough concave areas with chemical interaction between iron oxide and silica surface.

Deng (1997) studied the technique of precipitation from homogeneous solutions to simulate the formation of iron (Fe^{3+}) hydroxides occurring at the redox boundary of natural waters. The pathway of iron (Fe^{3+}) precipitation from

homogenous solution observed here was similar to the mechanism of the chemical processes occurring in natural pH which regulated largely by the carbonate system. The results showed that the formation of iron (Fe^{3+}) hydroxides was strongly influenced by inorganic species, i.e., either incorporated into the structure of the iron (Fe^{3+}) hydroxides or only affected the morphology without being integrated into the solid structure.

2.2.2 Heavy Metal Removal by Adsorption Process

Lai et al. (1999) developed process for coating hydrated iron oxide on the sand surface and attempted to utilize the adsorption property of the coating as well as the filtration property of the sand. The results indicated that the iron-coated sand had more micro pores and higher specific surface area because of the attachment of iron oxide. Copper ions could penetrate into the micro pores and mesopores of iron oxide on the sand surface. Besides, the results of EDAX analysis showed that copper ions were chemisorbed on the surface of iron-coated sand.

Lai and Chen (2000) investigated on metal ions and natural organic matters adsorption by iron-oxide coated sand in both batch and column operations. From the batch experiment, copper and lead ions could be removed simultaneously by the iron-coated sand in the competition adsorption manner. The interaction between copper, lead ions and iron oxide on sand surface was primarily the chemical bondings. The maximum capacity of iron coated sand for copper and lead were 0.259 mg Cu/g sand and 1.211 mg Pb/g sand, respectively. Results from column experiments indicated that the copper ions, lead ions and humic acid could be removed completely before

the breakpoint. As a result, the iron-coated sand may be successfully applied for the adsorption/filtration of metal ions and natural organic matters in water.

Lin and Chang (2000) used fly ash which containing metal oxides, carbon and other microelements to remove Cu^{2+} . Experimental results showed that the specific area of fly ash increased linearly with the quantity of carbon content. The carbon fraction in fly ash was important in the removal of Cu^{2+} at pH 5. However, Cu^{2+} removal owing to precipitation was increased with a decreasing carbon fraction and the contribution of copper precipitation was estimated to be approximately 23-82% of total removal, depending on the carbon fraction of the fly ash.

Le (2003) determined the method for preparing iron (III)-based binary oxide adsorbents in a granulated form and then applied to remove arsenic. The key step in the method was the simultaneous generation of hydrous ferric oxide (FeOOH) sol and silica sol in situ in one reactor. This eventually led to the formation of Fe-Si complexes. The addition of silica enhanced the granulated adsorbent strength but reduced the arsenic adsorption capacity. The effects of aging time, drying temperature, and process pH on adsorbents were also evaluated in the study. X-ray diffraction analysis confirmed that the iron (III) oxide in the Fe-Si binary oxide adsorbents was amorphous, largely due to the retardation of the iron oxide crystallization by the presence of silicate species. The surface area of the Fe-Si adsorbents and the particle size of Fe-Si complexed suspensions were determined as well. The batch strength testing procedure introduced in this study can provide a simple and quick evaluation of granulate strength in a wet status.

Lee et al. (2004) used a fluidized-bed reactor (FBR) filled with manganese-coated sand (MCS) to treat copper-contaminated wastewater. The adsorption

characteristics of MCS, the adsorption equilibrium of MCS, and the copper removal capacity by MCS in FBR were investigated. In terms of the adsorption characteristics of MCS, the surface of MCS was evaluated using a scanning electron microscope (SEM). Energy dispersive analysis (EDS) of X-rays indicated the composition of MCS, and the quantity of manganese on MCS was determined by means of acid digestion analysis. The experimental results indicated that copper was removed by both sorption (ion exchange and adsorption) and co-precipitation on the surface of MCS in FBR. Copper removal efficiency was highly dependent on the pH and increased with increasing pH from pH 2 to 8. After the copper adsorption by MCS, the pH in solution was decreased. The adsorption sites of MCS could be used efficiently by the FBR. A Langmuir adsorption isotherm equation was fitted with the measured adsorption data from the batch equilibrium adsorption test better than the Freundlich adsorption isotherm. In addition, the adsorption rate increased when the wastewater was aerated.

Hlavay and Polyák (2004) The adsorbent was prepared by in situ precipitation of $\text{Fe}(\text{OH})_3$ on the surface of activated Al_2O_3 as a support material. The total capacity of the adsorbent was 0.12 mmol/g, and the pH of zero point of charge (pH_{pzc}) was 6.9 ± 0.3 . Depending on the H^+ of solutions, the adsorbent can be used for binding of both anions and cations, if $\text{pH}_{\text{eq}} < \text{pH}_{\text{zpc}}$ anions are sorbed on the surface of adsorbent (S) through $\{\text{S}-\text{OH}^{+2}\}$ and $\{\text{S}-\text{OH}\}$ groups. A graphical method was used for the determination of pH_{iep} (isoelectric points) of the adsorbent and values of pH_{iep} was 6.1 ± 0.3 for As(III) and 8.0 ± 0.3 for As(V) ions. The amount of surface charged groups (Q) was about zero within the pH range of 6.5–8.6, due to the practically neutral surface formed on the adsorption of As(V) ions. The adsorption of arsenate

and arsenite ions from solutions of 0.1–0.4 mol/L was represented by Langmuir-type isotherms. A great advantage of the adsorbent is that it can be used in adsorption columns, and low waste technology for arsenic removal from drinking water can be developed.

Regarding on these literature reviews, characteristics of iron oxide coated media depend mainly on the physical and chemical conditions used for coating process. Therefore, iron coated media obtained from different processes tend to possess dissimilar properties including iron oxide species, specific coating capacity, adhering strength which directly relates to heavy metal sorption ability (Lo et al., 1997; Deng, 1997). The suitable pH for iron oxide precipitation was around neutral pH which can produce a large amount of iron oxide coating on media surface; hence, pH of 6.5 was used intensively through out this study. Nonetheless, acidic pH at 4.4 and basic pH at 12.0 were also employed for confirmation. Copper was used as a target metal for sorption experiment since it was widely used by many studies which, as a result, were available for comparison. With its aqueous solubility, the studied copper concentration of 63.5 mg/L or 1 mM was prepared at pH 6 which not provided any copper hydroxide precipitation. This concentration was also used by several other researchers such as Lai et al (1999), Lai and Chen (2000), Lin and Chang (2000); therefore, the sorption data obtained from this study can be conveniently compared to those mentioned papers.

CHAPTER III

METHODOLOGY

3.1 Materials

3.1.1 Seeding Materials

Quartz sand (SiO_2) and aluminum oxide (Al_2O_3) with the properties shown in Table 3.1 was used in this experiment. Both of media were pretreated in HCl solution (Merck KGaA, Germany) at pH 1 for 24 hr. Then, it was washed with deionized water (Millipore Simplicity, France) until pH in the solution equaled to 7, and oven dried at 103°C (Lo and Chen, 1997).

3.1.2 Fluidized Bed Reactor

A 1.3 L. of fluidized bed reactor (FBR) was operated in all experiments performed. The reactor was a glass cylinder reactor consisting of outlet, inlet and recirculate sections. The carriers were added in FBR and operated at the optimum bed expansion. The dimensions of fluidized bed reactor were 5 cm. diameters with 70 cm. of height illustrated as shown in Figure 3.1.

Table 3.1 Seeding Materials Properties

Chemical form	size (mm.)	Point of zero charge (PZC)
Al_2O_3	0.25	2.8
SiO_2	0.42 – 0.59	9.0

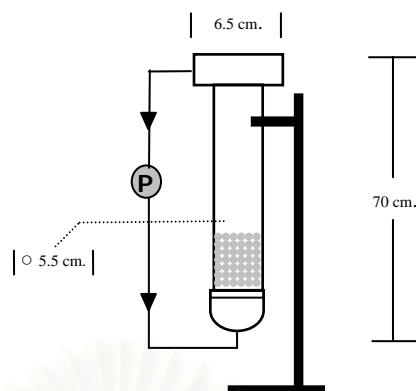


Figure 3.1 Schematic of fluidized bed reactors for iron pelletization.

The apparatus used in this experiment consists of two main components: a liquid-solid fluidized bed and three phase fluidized bed (gas-liquid-solid). The liquid-solid column is made up of a tall cylindrical column that contains seeding materials. To control bed expansion, it has a digital recirculate flow rate controller to maintain the bed expansion. The three phase fluidized bed is almost the same, except for ambient air was added at the bottom of column. Moreover, it has an analog pressure gauge to indicate the gas pressure that introduce through the column.

3.1.3 Chemicals

Fe^0 of 10 μm size (specific surface area $\approx 1 \text{ m}^2/\text{g}$) purchased from Merck KGaA, Germany was used without any pretreatment. The CO_2 gas with purity greater than 99.5% was obtained from a local supplier. 35% of hydrogen peroxide (H_2O_2) solution, 70% nitric acid (HNO_3) and sodium hydroxide (NaOH) were purchased from Merck KGaA Germany. Ambient air and Nitrogen gas was obtained from chemical supplier.

Batch adsorption experiments were conducted by using copper ion solution prepared from CuNO_3 (copper nitrate, Merck). 70% nitric acid (HNO_3), sodium hydroxide (NaOH) and NaNO_3 were ordered from Merck KGaA Germany.

3.2 Experimental Methods

All studies were conducted in a batch mode. To determine the effectiveness of specie-alteration technique (from Fe^{2+} to Fe^{3+}) on surface coating on seeding material, two methods have been used, i.e., Fenton pretreatment by H_2O_2 addition and ambient aeration pretreatment (three phase process). Figure 3.2 showed experimental diagram of this study.

3.2.1. Iron-Coated Sand Preparation

3.2.1.1. Fenton Pretreatment

This experimental part was obtained in a four-step procedure as showed in Figure7; 1) ferrous preparation by Fe^0/CO_2 process, 2) Fe^0 separation; 3) Fenton pretreatment; and 4) iron precipitation/crystallization by fluidized bed process. Ferrous solution was prepared by simulating Fe^0 corrosion in DI water using a cylindrical reactor of 1.3 liter. A peristaltic pump was used to circulate water within the column to provide sufficient mixing. CO_2 gas at 200 ml/min was introduced into

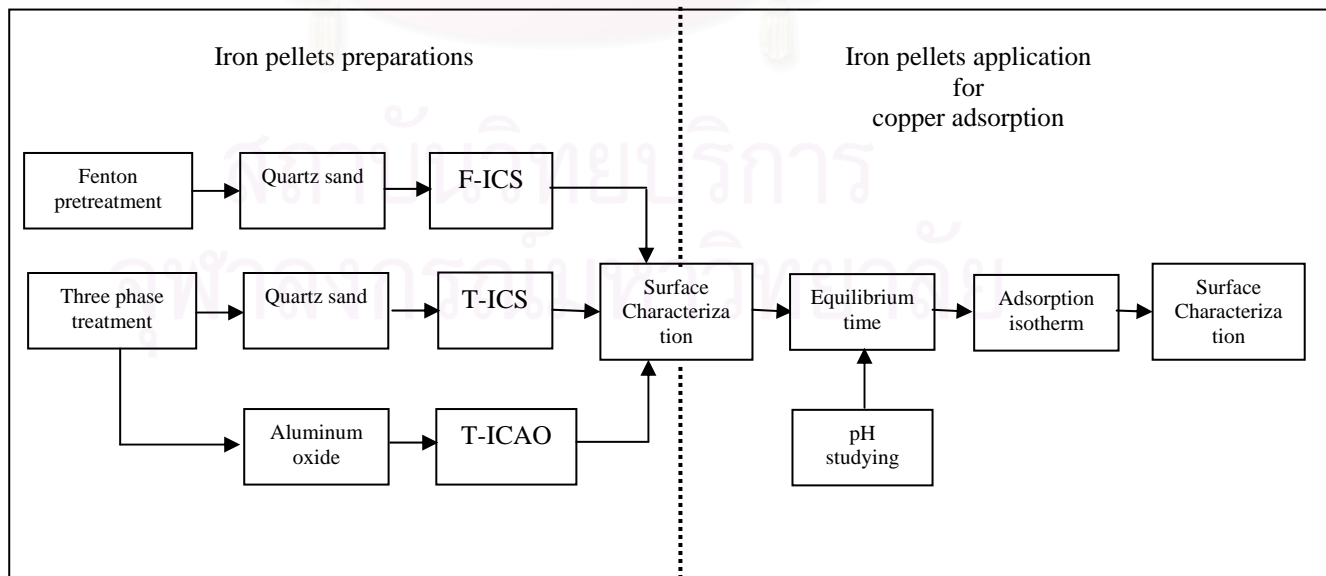


Figure 3.2 Experimental diagram of this study

the solution to maintain proper pH through a disk diffuser of silicate material installed at the bottom of the reactor. After 60 min of the reaction time, Fe^0 was settled for 30 min in the reactor which is covered with parafilm to prevent oxygen transfer from the atmosphere. Supernatant containing ferrous was withdrawn, checked for concentration, and kept without oxygen until being used. The initial ferrous concentration was varied by changing initial Fe^0 dosage.

In this Fenton-pretreatment scenario, Fe^{2+} was transformed to Fe^{3+} via Fenton reaction. Ferrous solution prepared previously was added with H_2O_2 and reacted for 2 min to generate Fe^{3+} by using a magnetic stirrer in a beaker. The 0.5 a molar ratio of $\text{Fe}^{2+}/\text{H}_2\text{O}_2$ was applied to ensure that Fe^{2+} is completely consumed whereas no H_2O_2 residual remains in the solution.

Finally, sand media was added into the reactor for the iron precipitation/crystallization. The diameter and height of the reactor are 5 and 70 cm, respectively. A recirculated pump is used to fluidize the sand bed. Desired pH was adjusted by NaOH. The samples were taken at desired intervals for total iron analysis. Besides, the adsorption characterizations of iron pellets were investigated. Sample were also be further analyzed by SEM and XRD.

3.2.1.2. Aeration Pretreatment

This iron oxide coating procedure is similar to that of Fenton pretreatment as mentioned earlier. The only difference is O_2 in the ambient air was supplied and served as an oxidant rather than H_2O_2 . Figure 3.3 showed the operation procedure in this scenario. The experiment was conducted in same manner as previous scenario in the first, second steps. Only the ambient air was used to change iron species from Fe^{2+} to Fe^{3+} in the third step by discharging directly into the fluidized bed reactor.

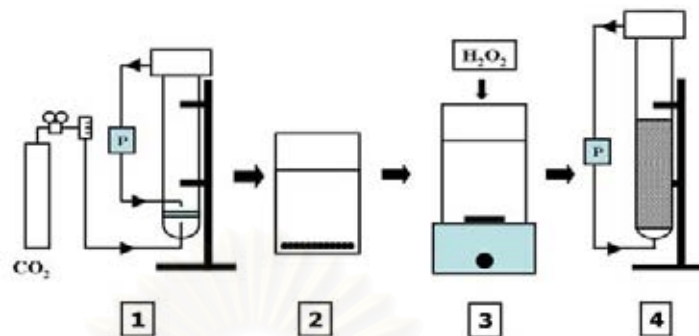


Figure 3.3 Operation procedures: 1) ferrous preparation by Fe^0/CO_2 , 2) settling Fe^0 separation; 3) Fenton pretreatment; and 4) iron precipitation/crystallization by fluidized bed process.

3.2.2 Acidic/Neutral/Alkaline Leaching Test

The objective of this part was to evaluate the amount of iron leaching from iron-coated pellet at different pH. DI water at different pH was added into 250 ml of flasks. Then, working solution was placed in an orbital shaker with the mixing intensity at 150 rpm. 4 g of each iron pellets were added into flask and covered with paraffin. 5 ml of solution sample was taken at different time interval and measured for pH. Total iron that leached into aqueous phase was analyzed by ICP.

3.2.3 Iron-Coated Aluminum Oxide Preparation

3.2.3.1 Three Phase Fluidized Bed Iron-Coated Aluminum Oxide

For quartz sand, the coating process followed the procedure that provided better results from Section 3.2.1. However, to improve the efficiency of iron coating onto aluminum oxide, some parameters such as initial pH, air flow rate, will be investigated to provide specific conditions which are suitable with aluminum oxide. Properties of iron-coated aluminum oxide will be examined similar to those in the case of quartz sand. Figure 3.4 showed the operation procedure of this part.

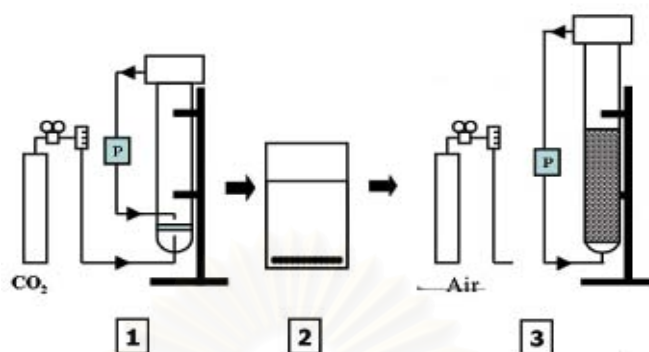


Figure 3.4 Three phase fluidized bed operation procedure: 1) ferrous preparation by Fe⁰/CO₂; 2) Fe⁰ separation; 3) iron precipitation by fluidized bed process.

3.2.4 Copper adsorption by iron pellet

Copper ion was prepared by dissolving appropriate amounts of Cu(NO₃). Batch adsorption experiments were conducted at pH 5.5 in 250 ml flasks. Initial concentrations of copper ions were held at 63.5 mg/l. All experiments were adjusted the background ionic strength to 0.1 N. 1 N of HNO₃ and 1 N of NaOH were used for pH adjustment. In terms of mixing condition, all flasks were rotated end-over-end at 150-154 revolutions per min. Adsorption equilibrium experiments were conducted by equilibrium an accurately weighted 4 g of iron pellets.

To evaluate how iron pellets dosage affects Cu (II) removal, 1, 2, 4 and 8 g of each type of iron pellets were added to the copper solution. The pH was monitored during the adsorption reaction and adjusted to required level at each sampling time, if necessary. Samples were taken at different time interval and filtered by 0.45 μm membrane. Besides, the morphology of iron pellets after copper adsorption was determined by SEM.

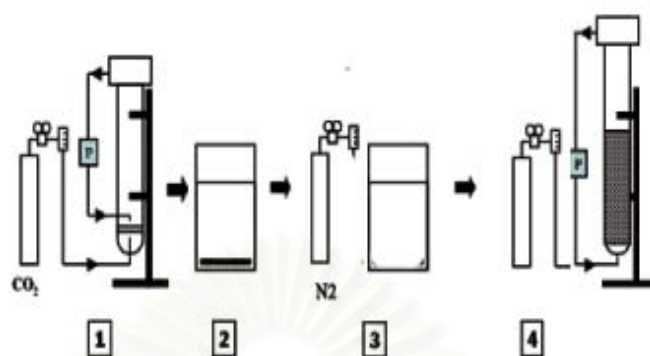


Figure 3.5 Operation procedures: 1) ferrous preparation by Fe^0/CO_2 ; 2) settling Fe^0 ; 3) adjusts pH by nitrogen purge; 4) iron precipitation by fluidized bed process.

3.3 Analytical Instruments

Fe^{2+} was able to form a colored complex with 1,10-phenanthroline; therefore, its concentration was determined by using the spectrophotometer (SHIMADZU, UV-1201, Japan) with the light wavelength set at 510 nm (Standard Methods, 1995). Total iron and copper was analyzed by inductively couple plasma or ICP-AES (ICP) (JY2300, MLS-1200, and Milestone, Italy). Micro-morphology and the surface composition of the iron pellets were obtained by scanning electron microscopy coupled with energy-dispersive x-ray spectrometry (SEM-EDS, Hitachi S-3000N, Japan, EDS detector: HORIBA MOBEL 7021-H). Iron species of each iron pellets were identified by XRD (X-ray diffractometer, BRUKER axs, D8 advance). In addition, the solution pH was monitored continuously by using a pH meter (Suntex, TS-1, Taiwan).

CHAPTER IV

RESULTS AND DISCUSSION

4.1 Iron Pellets Preparation

4.1.1 Iron Coated Sand (ICS)

4.1.1.1 Fenton Pretreatment

A. Effect of Initial pH on Iron Coating onto Sand Surface in Fluidized Bed Process

In order to investigate the effect of initial pH on the iron precipitate/crystallization to media, the initial pH was imposed at 4.4, 6.5, and 12.0. The results in Figure 4.1 showed that the iron removal at 5 hrs was 36.8%, 96% and 76.4%, respectively. The final pH of working solution did not or only slightly changed from the initial values, i.e., 4.9, 6.7 and 12.0, respectively. The results showed that pH played an important role on the iron removal in the fluidized bed process with the optimum value at 6.5. According to the pC-pH diagram for hydrolysis products of Fe^{3+} (Figure 4.2), the lowest solubility of $\text{Fe}(\text{OH})_3$ is found around neutral pH and the predominant soluble specie is either $\text{Fe}(\text{OH})_2^+$ or $\text{Fe}(\text{OH})_4^-$. Since the data obtained in this study agree very well with $\text{Fe}(\text{OH})_3$ precipitation equilibria, it suggests that the specie of iron on coated sand in this Fenton pretreatment (F-ICS) should be $\text{Fe}(\text{OH})_3$ rather than other iron oxide species. This hypothesis is firmly supported by the result from XRD analysis which identified the coating specie to be mainly $\text{Fe}(\text{OH})_3$ as shown in Figure 4.3

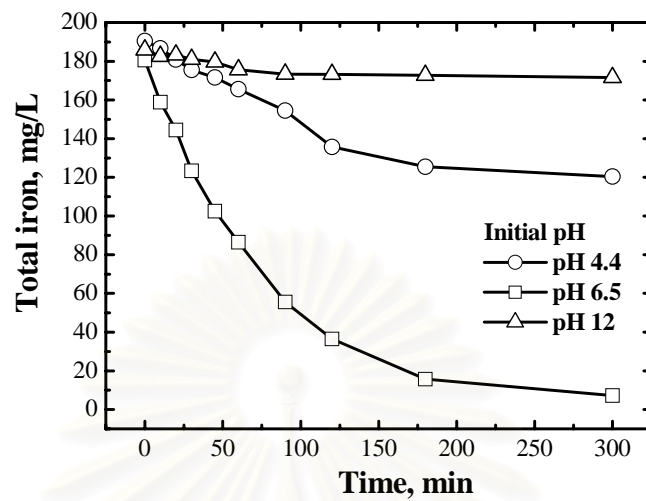


Figure 4.1 Effect of pH on the iron removal in fluidized bed process. (Initial iron concentration was 185 mg/L. The amount of sand dosage used in these experiments was 300 g/L. The bed expansion was controlled at 0.5 from the original bed level. The varying of initial pH was 4.4, 6.5 and 12)

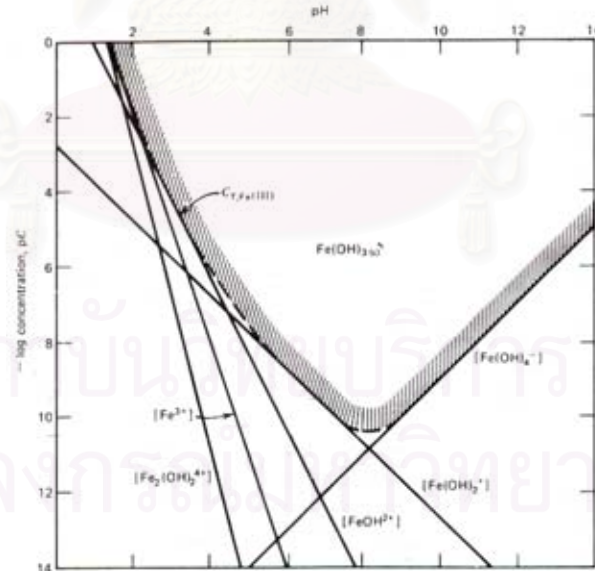


Figure 4.2 pC-pH diagram for hydrolysis products of Fe^{3+} (Snoeyink and Jenkins, 1980).

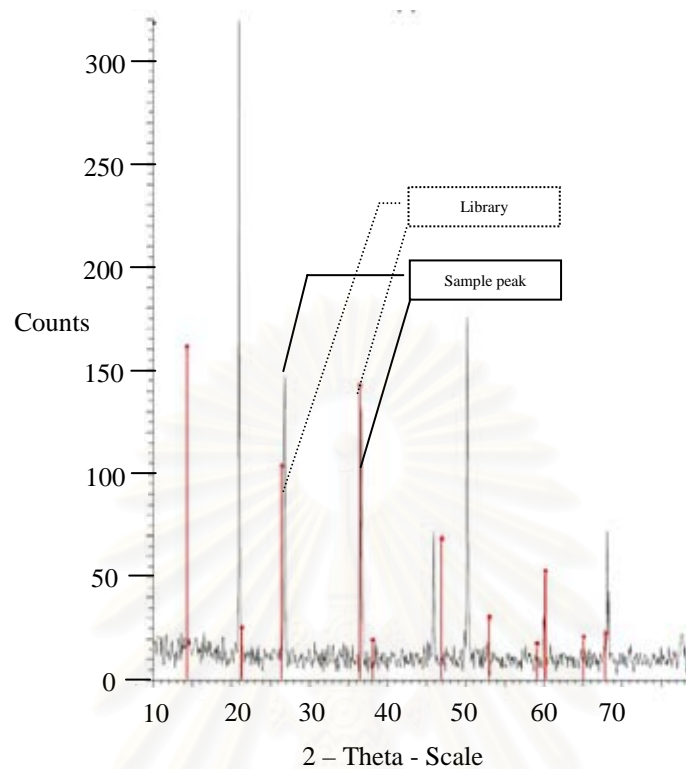


Figure 4.3 Characteristics of fenton pretreated iron coated sand (F-ICS) by XRD analysis.

B. Effect of Recirculation Flow Rate on Iron Coating onto Sand surface in Fluidized Bed Process

Figure 4.4 exhibited the impact of flow rate on iron removal in fluidized bed process. The bed expansion was controlled at 0.5, 0.75, and 1.0 by setting the recirculation flow rate at 2,100, 2,700, and 3,300 ml/min, respectively. The initial iron and sand dosages of 185 mg/L and 300 g/L, respectively, were used in this study at the pH of 6.5 which found to be the optimum value from previous section. The results showed that the lower bed expansion tended to provide higher iron removal. At the bed expansion of 0.5, 0.75, and 1.0, the 5-hour removal of ferric were 70, 60, and 50%, respectively. The low iron removal at high bed expansion was possibly referred to the shear force between iron hydroxide and sand surfaces. High flow rate produced turbulent flow and created excessive shear force which made iron solid hard

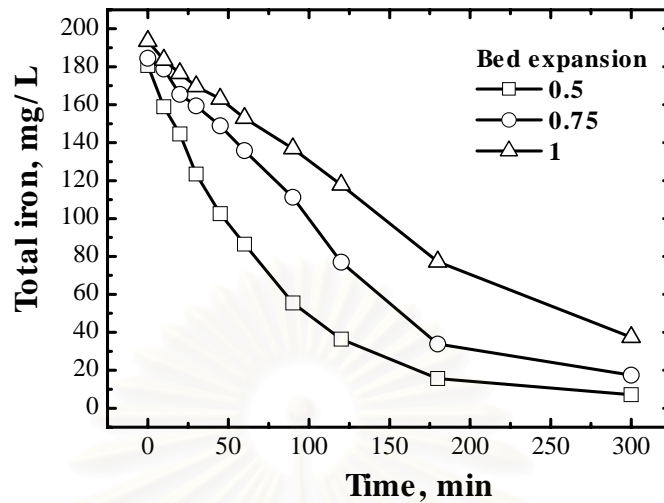


Figure 4.4 Effect of flow rate on the iron removal in fluidized bed process. (Initial iron concentration was 185 mg/L. The amount of sand dosage used in these experiments was 300 g/L. The bed expansion was varied at 0.5, 0.75 and 1 from the original bed level. The initial pH was set at 6.5)

to coat onto the sand surface. Therefore, the suitable hydraulic condition for iron pelletization on sand in fluidized bed process should be laminar flow or low turbulent.

C. Effect of Sand Dosage on Iron Coating onto Sand Surface in Fluidized Bed Process

Regarding the effect of sand dosage on the iron removal in fluidized bed process, Figure 4.5 shows four different sand dosages of 200, 300, 400, and 500 g/L at 0.5 bed expansions. Specific conditions were provided at total iron concentration of 185 mg/L and initial pH of 6.5. It was interesting to find out that the iron removal was increased with the increasing sand dosage until reaching a plateau where an additional amount of sand did not provide a better outcome. With the sand dosage of 200 g/L and 300 g/L, the iron removal was 63% and 80% at 2 hrs and by 85% and 96% at 5 hrs, respectively. As the sand dosage increased up to 400 and 500 g/L, the

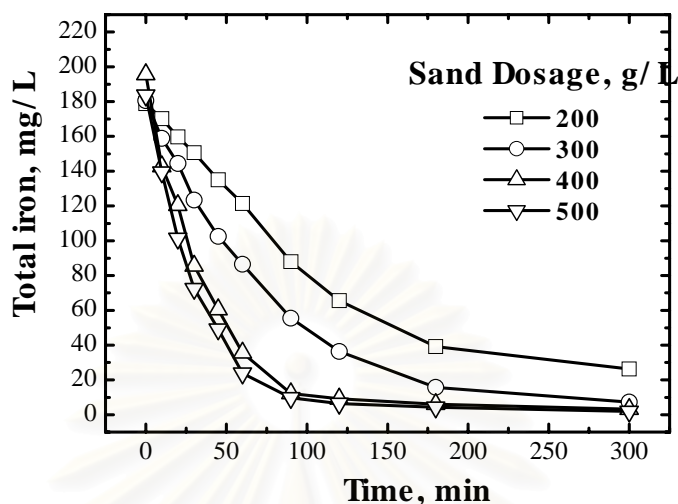


Figure 4.5 Effect of sand dosage on the iron removal in fluidized bed reactor. (Initial iron concentration was 185 mg/L. The amount of sand dosage used in these experiments was varied from 200, 300, 400 and 500 g/L. The bed expansion was controlled at 0.5 from the original bed level. The initial pH was set at 6.5)

removal efficiencies increased to 98 and 99% at 2 hrs. According to kinetic analysis, all obtained data were able to explain with the first order reaction (graphical determination was showed on appendix B). In general, the surface reaction in water is governed by two-sequential-step mechanism, i.e., a) transport through water film layer and diffusion into the pores; and b) reaction at the surface. Since aluminum oxide and silica oxide have very smooth surface with negligible porosity (discussed later), pore diffusion can be neglected. In addition, previous section has shown that the fluidization with 0.5 bed expansion could remove iron better than 0.75 and 1.0 expansion; hence, it implies that the liquid film thickness was already minimized at 0.5 bed expansion. Therefore, the mass transport step should not be a limiting step for iron removal under the conditions used in this study. Morel and Hering (1993) state that the surface reaction process can be described by a bimolecular reversible chemical reaction:



$$\text{hence} \quad d[C]/dt = -k_f[\equiv X][C] + k_r[\equiv XC] \quad (4.2)$$

where: “ $\equiv X$ ” is the reactive size on the carriers and “C” is the target compound. In this study, either aluminum oxide and silica oxide was used in an excess amount as compared to iron concentration; hence, the reactive size can be presumed constant. Furthermore, the results from leaching test which will be discussed later showed that less than 1% of coated iron was leached out from the solid phase. This implies that the reversible reaction in equation (4.1) is insignificant. Thus, the rate law in equation (4.2) is simplified to be:

$$d[C]/dt = -(k_f[\equiv X])[C] \quad \text{or} \quad = -k_f'[C] \quad (4.3)$$

Equation (4.3) is very consistent with the findings of this study in which the iron removal rate could be explained by first-order reaction. The rate constants are listed in Table 4.1 which indicating that the rate constant was increased with increasing sand dosages. The effect of sand dosage on iron removal in fluidized bed process was considered to be due to the greater specific area for iron precipitation with the increasing of sand dosage. However, applying sand in an excess amount was not necessary leading to the efficiency improvement.

D. Effect of Ferric Concentration on Iron Coating onto Sand in Fluidized Bed Process

To further understand the effect of initial ferric concentration on the iron precipitation by fluidized bed process, ferric concentration was varied from 126 to 188, 252 and 334 mg/L, respectively. Specific conditions were provided at initial pH

Table 4.1 First-order rate constants for iron removal at various ferrous concentrations and sand dosages in fenton pretreated fluidized bed process.

[Fe ²⁺] (mg/L)	Sand dosage (g/L)	k, ×10 ⁻³ (1/hr)	R ²
126	400	41.6	0.95
189	200	7.10	0.97
189	300	11.8	0.99
189	400	27.4	0.98
189	500	30.1	0.98
259	400	7.4	0.99
334	400	6.4	0.97

6.5, 400 g/L of sand dosage and bed expansion at 0.5. The iron removal profiles with different initial ferric concentration were presented in Figure 4.6. It showed that iron was removed at 97 and 95% within 120 min for the initial ferric concentration of 126 and 188 mg/L. In contrast, at concentrations of 252 and 334 mg/L, residual total irons at 300 min were 54.2 (78% removed), and 82.3 mg/L (75% removed), respectively. The first-order rate constants decreased with increasing initial iron concentration as shown in Table 4.1. Deterioration in removal efficiency may possibly due to surface limit on sand particles; hence, iron solid form could not attach to the sand surface and as a consequence, suspended in the liquid phase and left the sand bed. However, the iron residue at the initial iron concentration of 252 and 334 mg/L might be lower at longer reaction period.

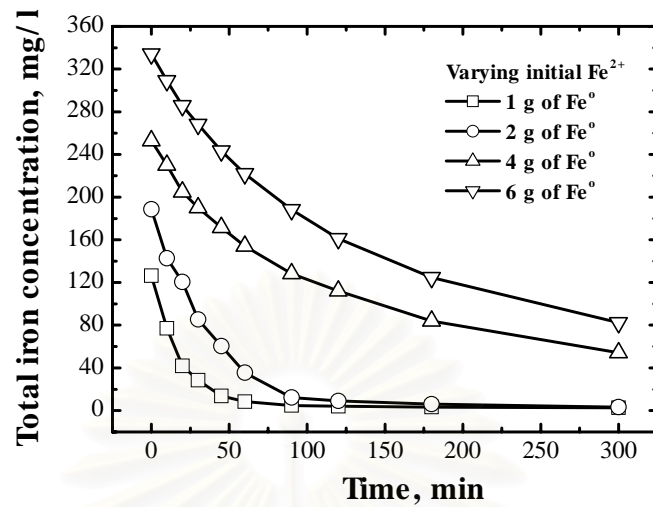


Figure 4.6 Effect of initial iron concentration on the iron removal in fluidized bed process. (Initial iron concentration was 126, 188, 252 and 334 mg/L. The initial pH was set at 6.5. The amount of sand dosage was 400 g/L and bed expansion was controlled at 0.5)

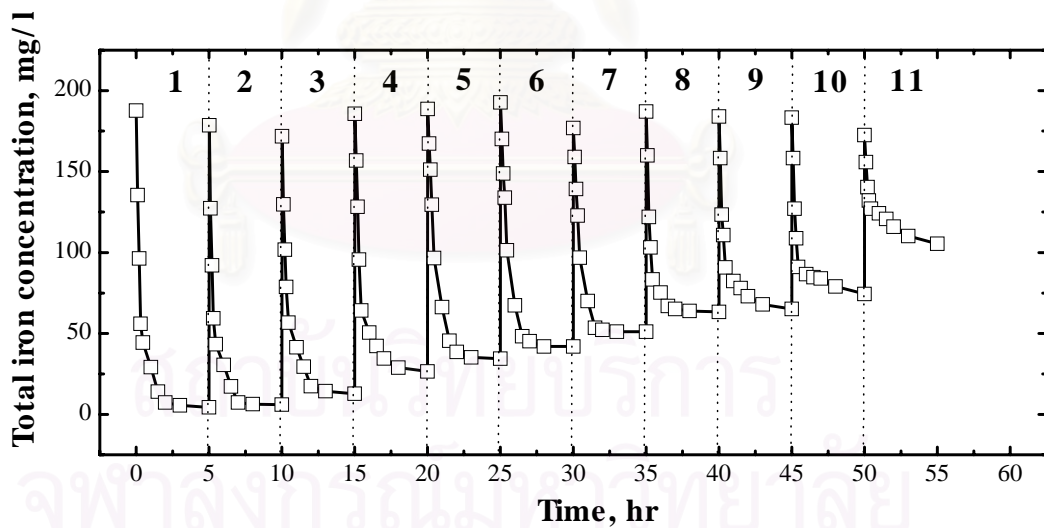


Figure 4.7 Repeatability of sand for iron removal efficiency. (Initial sand dosage and iron concentration were 400 g/L and 185 mg/L, respectively, with 0.5 bed expansion and pH of 6.5. Treated solutions from the previous phase were emptied and filled in with fresh iron solution. Sand was reutilized for iron removal)

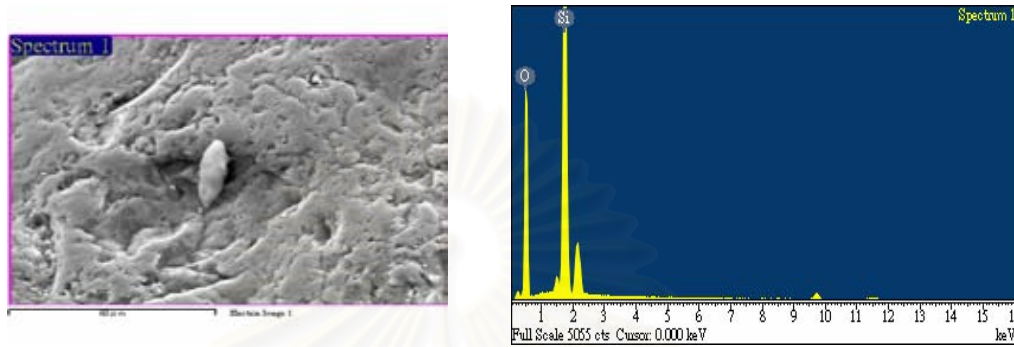
E. Repeatability of Sand for Iron Removal.

Sand repeatability test was achieved by sequential batch experiment. Newly prepared Fenton-pretreated ferric solutions were repeatedly passed through the fluidized-bed reactor. Figure 4.7 showed that the iron removal efficiency decreased with increasing the batch operation. As can be seen, the residual iron concentration rises gradually and constantly in the later batches. It is suggested that available surface area for iron attachment was reduced as sequential batch experiment proceeded.

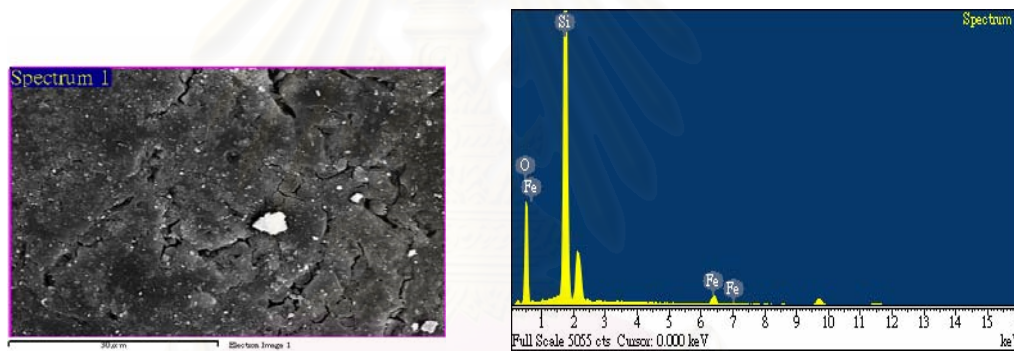
Regarding on physical appearance of sand surface, the sand grain color changed from originally white-gray to light brown after the first batch experiment. Then, it became darker and darker as the sequential batch operation was conducted. Morphology comparison between fresh and used sands was illustrated in Figure 4.8. The surface of fresh sand was smooth and had relatively lower porosity (Figure 4.8 (a)). However, the sand surface changed dramatically after iron coating took place from run to run as shown in Figure 4.8(b), i.e., became rugger and rugger afterward. After 11 batches, the surface of F-ICS became even more different from that of fresh sand (Figure 4.8(c)). In accordance with surface composition analysis by SEM-EDS presented in Table 4.2, the weight percentage of iron increased with increasing number of batch operation. The percentage of iron coated on sand surface after 11 batch operations increased up to 25.75% which was much larger than that with the fresh sand of 0.2%. In addition, the measurement of total iron showed that the amount of iron coated per unit weight of sand increased from 0.45 mg Fe/g sand with the first batch to 3.56 mg Fe/g sand in the 11th batch. The recovery was 95% based on calculation from iron removal within eleven batch operations. The maximum iron

coating capacity of sand can be used to predict the appropriate time for replacing the used sand with the fresh one, in view of process operation.

(a)



(b)



(c)

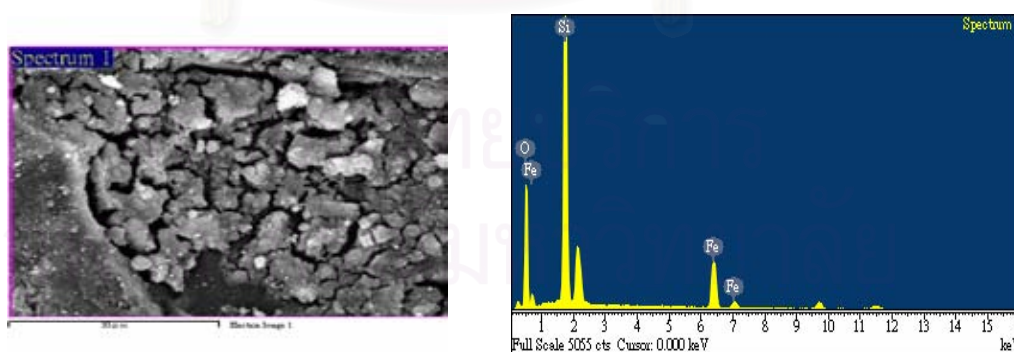


Figure 4.8 Surface morphology and EDS spectrum of F-ICS by SEM and EDS:
 (a) fresh sand, (b) F-ICS from batch 1; (c) F-ICS from batch 11.

Table 4.2 Surface composition of sequential batch of F-ICS by SEM-EDS.

Element	Fe	Si	O	Total
	% Weight	% Weight	% Weight	% Weight
Fresh sand	0.2	52.95	46.85	100
1st batch	3.27	50.18	46.55	100
3rd batch	10.77	37.81	51.42	100
5th batch	22.51	36.73	40.76	100
7th batch	21.74	41.00	37.25	100
9th batch	25.19	38.84	35.97	100
11th batch	25.75	38.72	35.52	100

4.1.1.2 Aeration Pretreatment

A. Effect of Air Flow Rate on Iron Coating onto Sand Surface in Three-Phase Fluidized Bed Process.

To investigate the effect of air flow rate on iron precipitation in three phase fluidized bed process. The pH coating in this study was operated at 5.5 which was the pH of the effluent from Fe⁰/CO₂ process. The air flow rate was imposed at 20, 100, 300 and 500 ml/min. Meanwhile, the ferrous residual was analyzed as a function of time with different air flow rate. The result in Figure 4.9 demonstrated that the iron rapidly decreased at the first stage until 70 min and then became steady afterward. The percent removal of iron at 5 hrs was 95%, 90%, 88% and 81% at 20, 100, 300 and 500 ml/min, respectively. According to the ferrous oxidation by aeration, the higher amount of air flow rate tended to provide a higher ferric conversion (equation 2.19). However, these ferric species needed to be palletized onto sand surface

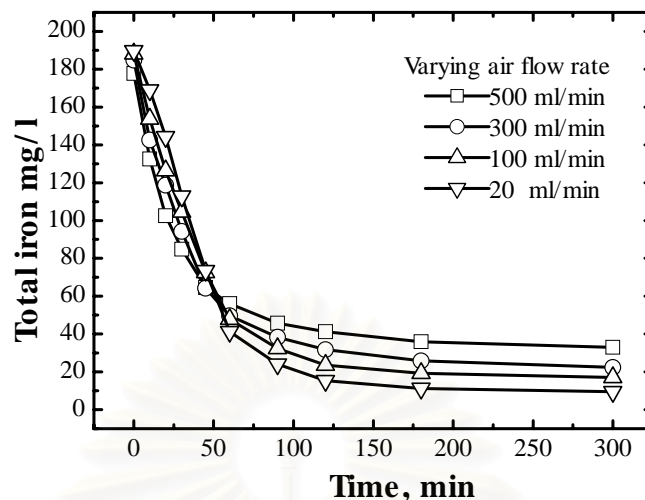


Figure 4.9 Effect of air flow rate on the iron removal in fluidized bed process. (The initial iron concentration was 185 mg/L. The amount of sand dosage used in these experiments was 400 g/L. The bed expansion was fixed at 0.5 from the original bed level. The initial pH was controlled at 5.5. The air flow rate was varied at 20, 100, 300 and 500 ml/min)

in order to be removed from aqueous phase. As the air flow rate increased, the shear force became amplified; hence, reduce pelletization efficiency.

In addition, the three phase iron coated sand (T-ICS) characterizations were also examined. The XRD analysis revealed that major iron-coating specie was mainly goethite, $\text{FeO}(\text{OH})$ as shown in Figure 4.10. The results from SEM on the surface morphology comparison between fresh and both kinds of iron coated (F-ICS and T-ICS) were illustrated in Figure 4.11. The surface of fresh sand was smooth and had relatively lower porosity (Figure 4.11 (a)). However, the sand surface changed dramatically after iron coating took place by pelletization process as showed in Figures 4.8(b) and 4.8(c). In accordance with surface composition analysis by SEM-EDS presented in Table 4.3, the weight percentage of iron increased after coating operation. The percentage of iron coated on sand surface after one batch operation of F-ICS and T-ICS were 3.27% and 1.90%, respectively. Furthermore, the measurement

of total iron showed that the amount of iron coated per unit weight of sand for F-ICS was 0.450 mg Fe/g sand and 0.431 mg Fe/g sand for T-ICS.

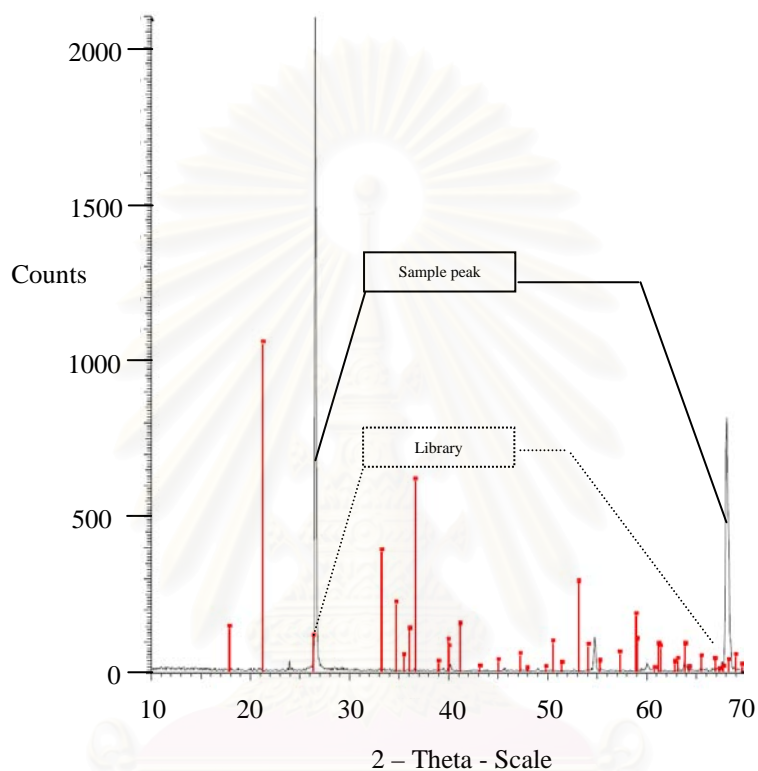


Figure 4.10 Characteristics of three phase iron coated sand (T-ICS) by XRD analysis.

Table 4.3 Surface composition of F-ICS and T-ICS by SEM-EDS.

Element	Fe	Si	O	Total
	% Weight	% Weight	% Weight	% Weight
Fresh sand	0.2	52.95	46.85	100
1 st batch F-ICS	3.27	50.18	46.55	100
1 st batch T-ICS	1.90	55.13	42.97	100

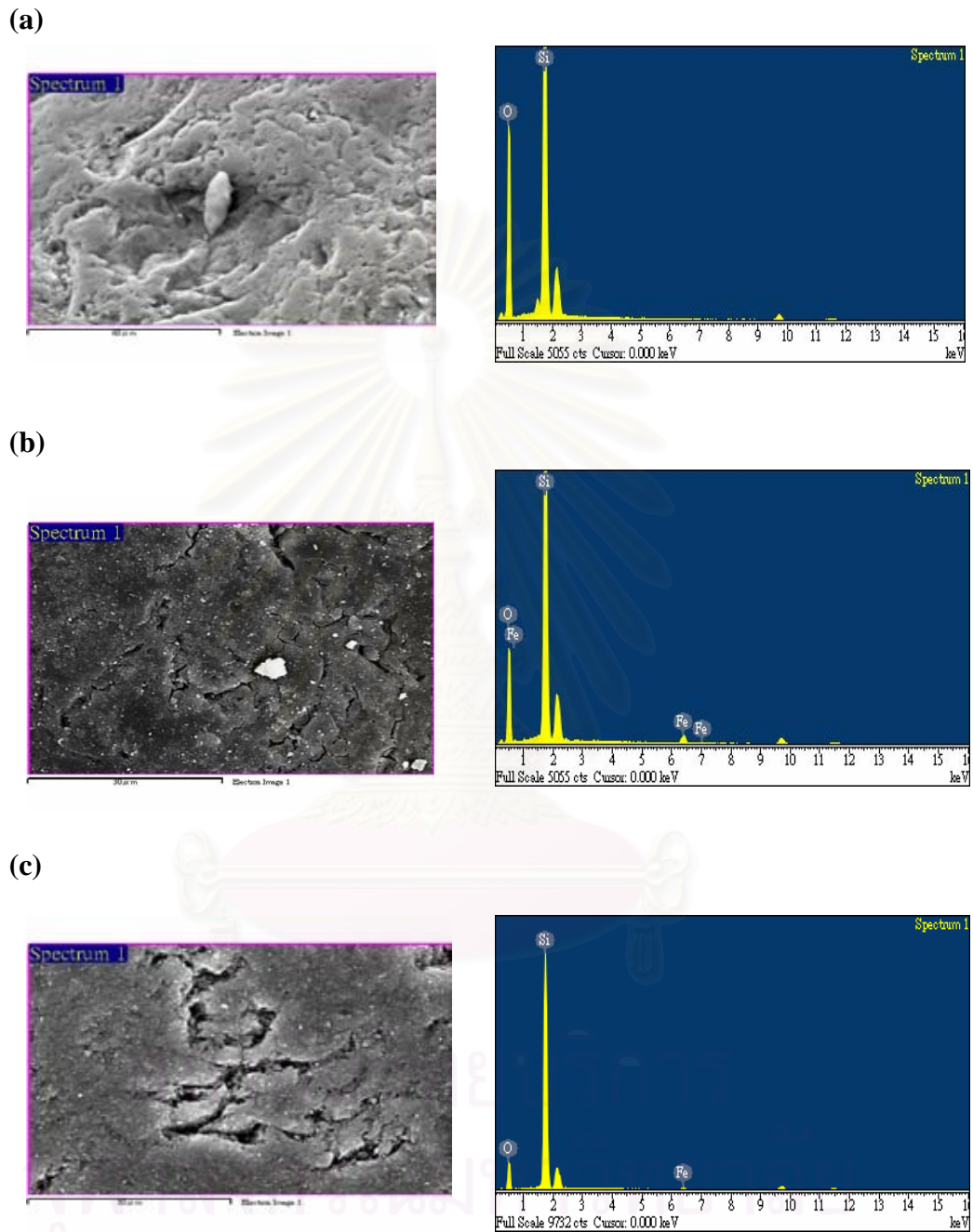


Figure 4.11 Surface morphology and EDS spectrum comparisons of ICS by SEM and EDS: (a) fresh sand, (b) 1st F-ICS; (c) 1st T-ICS.

B. Effect of Sand Dosage on Iron Coating onto Sand Surface in Three phases Fluidized Bed

Regarding the effect of sand dosage on ferrous removal in the fluidized bed reactor, the results were shown in Figure 4.12 under four different sand dosages of 200, 300, 400 and 500 g/L with the bed expansion ratio of 0.5. The total ferrous concentration was 185 mg/L. The air flow rate was controlled at 20 ml/min. As may be expected, the ferrous removal increased with increasing sand dosage similar to the Fenton pretreatment scenario. With the sand dosage of 200 g/L and 300 g/L, the iron removal was 63% and 82% at 2 hrs, and 83% and 91% at 5hrs, respectively. As the sand dosage increased up to 400 and 500 g/L, Fe^{2+} was removed by 94% and 95% at 2 hrs, respectively.

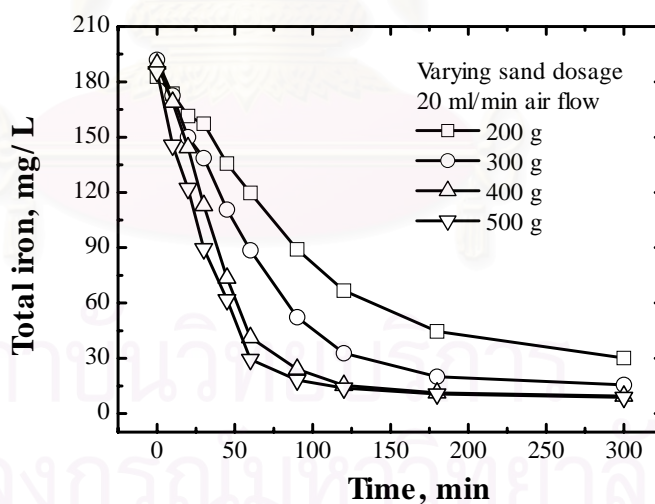


Figure 4.12 Effect of sand dosage on the iron removal in fluidized bed process. (The initial iron concentration was 185 mg/L. The bed expansion was fixed at 0.5 from the original bed level. The air flow rate was controlled at 20 ml/min. The initial pH was controlled at 5.5. The sand dosage was varied at 200, 300, 400 and 500 ml/min)

It is interesting to observe that the residual iron was only slight difference between the sand dosages of 400 g/L and 500 g/L.

The data was obtained from the effect of sand dosage on iron removal confirmed with previous study. Dosage of 400 g/L of sand was sufficient to remove 185 mg/L of initial iron concentration within 2 hrs at optimum operation for three phase fluidized bed process.

4.1.2 Iron Coated Sand Leaching Tests

In order to investigate the attachment strength of iron coated sand (F-ISC and T-ISC). Iron pellets obtained from the previous parts were leached with various conditions. The pHs used in this part were 3, 5, 7, 9, and 12 (acidic/neutral/basic condition). 4 g of iron coated sand was tested in 50 ml of solution. Figure 4.13 and Figure 4.14 showed the profiles of iron leaching from F-ICS and T-ICS to the solution at 72 hrs. For F-ICS case, the iron was leached from media rapidly at pH of 3, 5, 9, and 12 then, it gradually constant after 10 hrs, except at pH 7 in which iron leaching was minimal for F-ICS application. On the other hand, for T-ICS, the leaching of iron was diminutive and comparable at pH 5, 7, and 9.

The comparisons in term of amount of iron leaching per unit weight and leaching percentage between F-ICS and T-ICS was reported in Table 4.4, it suggests that the application of T-ICS can be conducted at the wider pH range than F-ICS.

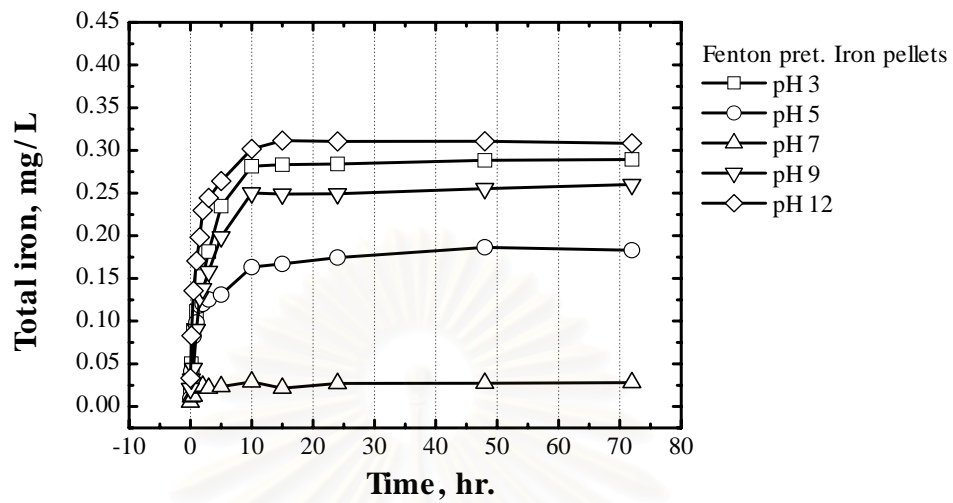


Figure 4.13 F-ICS leaching test as a function of time. (4 g of iron coated sand was tested in 50 ml of solution in experiment. The solution was varied at pH 3, 5, 7, 9, and 12).

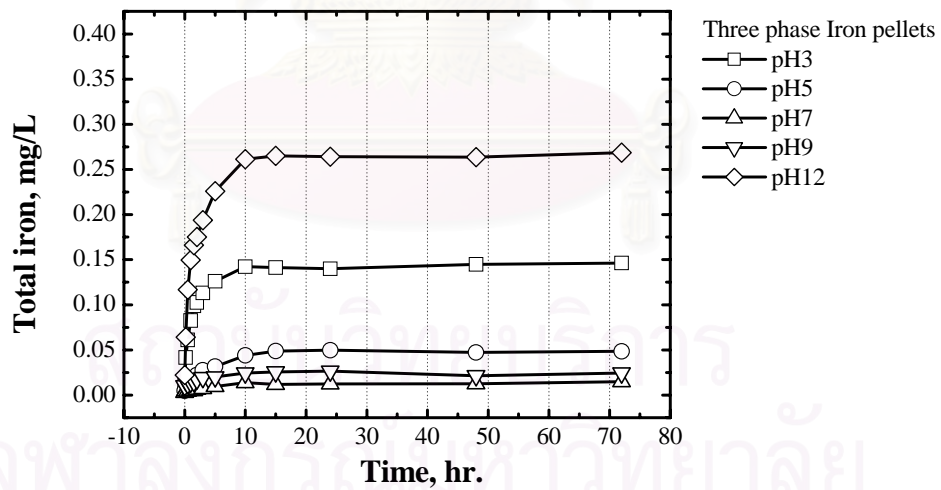


Figure 4.14 T-ICS leaching test as a function of time. (4 g of iron coated sand was tested in 50 ml of solution in experiment. The solution was varied at pH 3, 5, 7, 9, and 12)

Table 4.4 Comparisons of percent leaching between F-ICS and T-ICS at 72 hours.

pH	Fenton ICS			Three phase ICS		
	Amount of iron coated sand (mg Fe/g sand)	Amount of iron leaching (mg/l)	% leaching	Amount of iron coated sand (mg Fe/g sand)	Amount of iron leaching (mg/l)	% leaching
3	0.4568	0.0724	0.79 %	0.4305	0.0366	0.42 %
5		0.0458	0.50 %		0.0122	0.14 %
7		0.0070	0.08 %		0.0037	0.04 %
9		0.0651	0.71 %		0.0062	0.07 %
12		0.0771	0.84 %		0.0671	0.78 %

4.1.3 Iron Coated Aluminum Oxide (ICAO)

4.1.3.1 Aeration Pretreatment

As already mentioned, a coating process for this part was followed the procedure which provides better results in the case of quartz sand. The results from iron leaching test and application of ICS for the removal of copper (result showed in topic 4.1.4) were reported the iron coated sand which obtained from three phase fluidized bed process trends to provide better results. T-ICS was a lower percent of iron leaching at the same pH when compare with F-ICS include it can be apply at a wider pH range. Moreover, heavy metals as copper ion was removed by T-ICS effectively (explain in topic 4.1.4) However, to improve the efficiency of iron coating

onto aluminum oxide, some parameters such as initial pH, will be investigated to provide specific conditions which are suitable with aluminum oxide

A. Effect of Initial pH on the Iron Coating onto Aluminum Oxide Surface in Three Phase Fluidized Bed Process.

To investigate the suitable pH for iron coating onto aluminum oxide, the initial pH was imposed at 5.5 and 6.5. The results in Figure 4.15 showed that the iron removal at 5 hrs was 81%, and 91%, respectively. The final pH of working solution was increased slightly to 6.56, and 6.96, respectively. The results showed that pH played an important role on the iron removal in three phase fluidized bed process with the optimum value at 6.5.

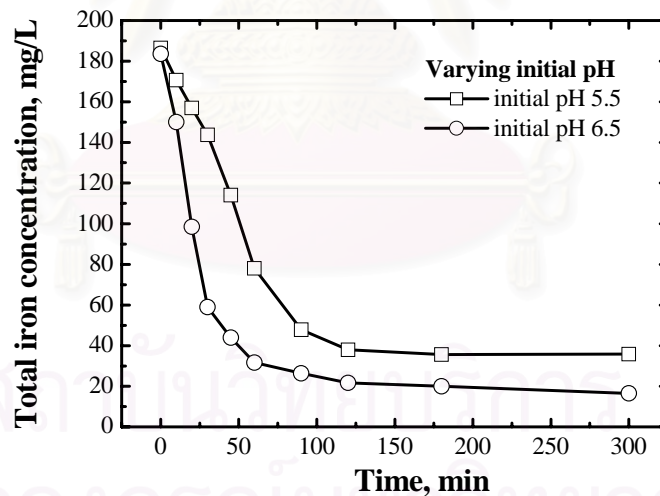


Figure 4.15 Effect of pH on the iron removal in fluidized bed process. (The initial iron concentration was 185 mg/L. The amount of aluminum oxide dosage used in these experiments was 400 g/L. The bed expansion was controlled at 0.5 from the original bed level. The varying of initial pH was 5.5 and 6.5)

Moreover, the three phase iron coated Aluminum oxide (T-ICAO) characterizations was studied. XRD analysis which identified the coating specie to be mainly iron oxide (Fe_2O_3) as shown in Figure 4.16. The result from SEM showed that surface morphology comparison between fresh, three phase iron coated aluminum oxide (T-ICAO) and three phase iron coated sand (T-ICS) as illustrated in Figure 4.17. The surface of fresh aluminum oxide was smooth and had relatively lower porosity (Figure 4.17(a)). Though, the aluminum oxide surface changed dramatically after iron coating took place as showed in Figure 4.17(b), the surface of T-ICAO at the end of the experiment became even different from that of fresh aluminum oxide.

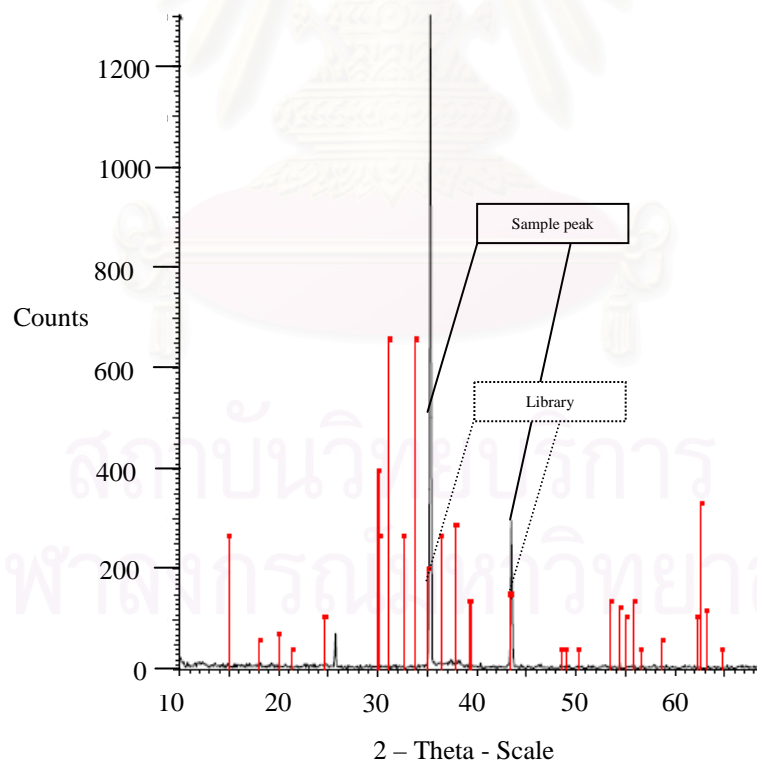
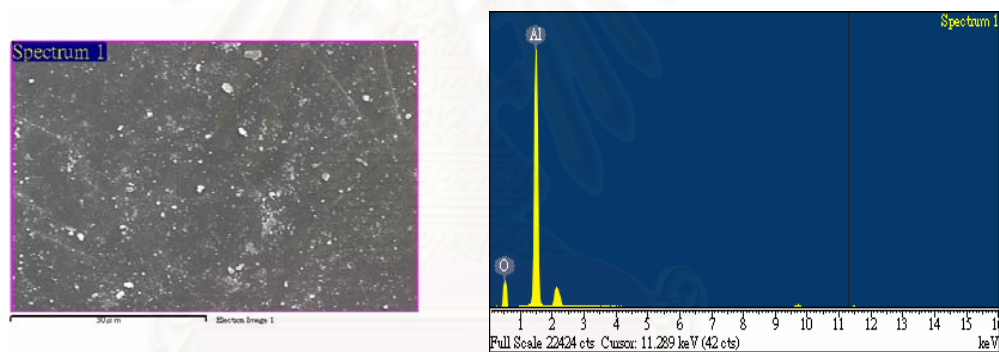


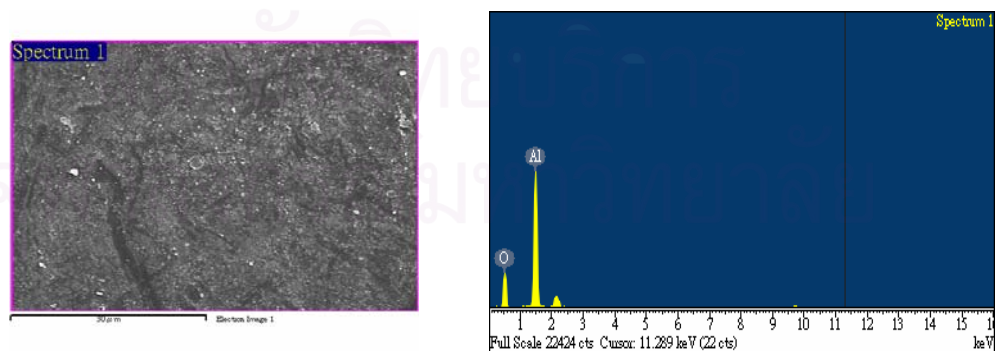
Figure 4.16 Characteristics of three phase iron coated aluminum oxide (T-ICAO) by XRD analysis.

Nevertheless, T-ICAO morphology was less roughness than T-ICS (Figure4.17(C)). In accordance with surface composition analyzed by SEM-EDS as presented in Table 4.5, the weight percentage of iron increased after coating operation. The percentage of iron coated on aluminum oxide surface after pelletization process was 1.01% which less than the percentage of iron on T-ICS (1.90%) Furthermore, the measurement of total iron showed that the amount of iron coated per unit weight of aluminum oxide was 0.417 mg Fe/g aluminum oxide which slightly different with I-CS (0.431 mg Fe/g sand).

(a)



(b)



(c)

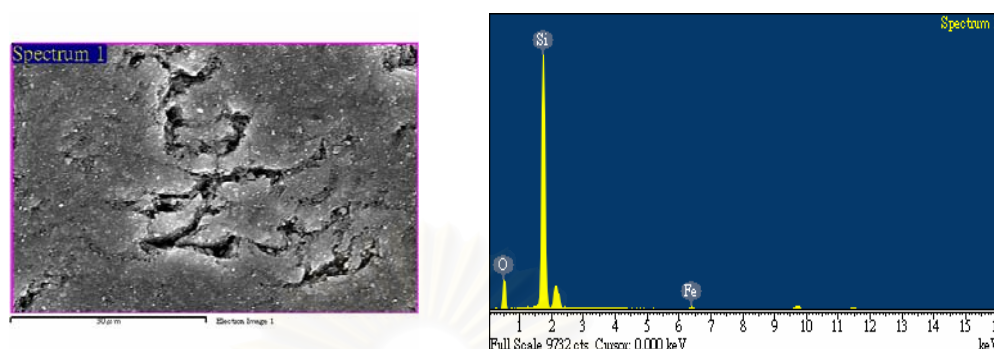


Figure 4.17. Surface morphology and EDS spectrum comparisons of ICS by SEM and EDS: (a) fresh Al_2O_3 , (b) T-ICAO; (c) T-ICS

Table 4.5 Surface composition of F-ICS and T-ICS by SEM-EDS.

Element	Fe	Si	Al	O	Total
	% Weight	% Weight	% Weight	% Weight	% Weight
Fresh Al_2O_3	0.00	-	50.80	49.20	100
T-ICAO	1.01	-	47.53	51.46	100
T-ICS	1.90	55.13	-	42.97	100

B. Effect of Aluminum Oxide Dosage on Iron Coating onto Aluminum Oxide Surface in Three-Phase Fluidized Bed Process

To study how aluminum oxide dosage affects on iron removal in three-phase fluidized bed process, four different aluminum oxide dosages of 200, 300, 400 and 500 g/L were employed. The experimental conditions were as follows: bed expansion ratio of 0.5, total ferrous concentration of 185 mg/L, initial pH of 6.5, and air flow rate of 20 mL/min. As may be expected, the ferrous removal increased with

increasing sand dosage as shown in Figure 4.18. With the sand dosage of 200 g/L and 300 g/L, the iron removal was 27% and 60% at 2 hrs, and 30% and 65% at 5 hrs, respectively. With the dosage increased up to 400 and 500 g/L, Fe^{2+} was removed by 90% and 92% at 3 hrs, respectively. Interestingly, the observation of residual iron was slight difference between the aluminum oxide dosages of 400 g/L and 500 g/L. As mentioned above, the higher amounts of material provide a greater specific area for iron precipitation. However, applying dose up to 500 g/L was in excess amount and not really improved the efficiency. Regarding to this part, 400 g/L of aluminum oxide was sufficient to remove 185 mg/L of initial iron within 3 hrs under the optimum process operation of three-phase fluidized bed process as described before.

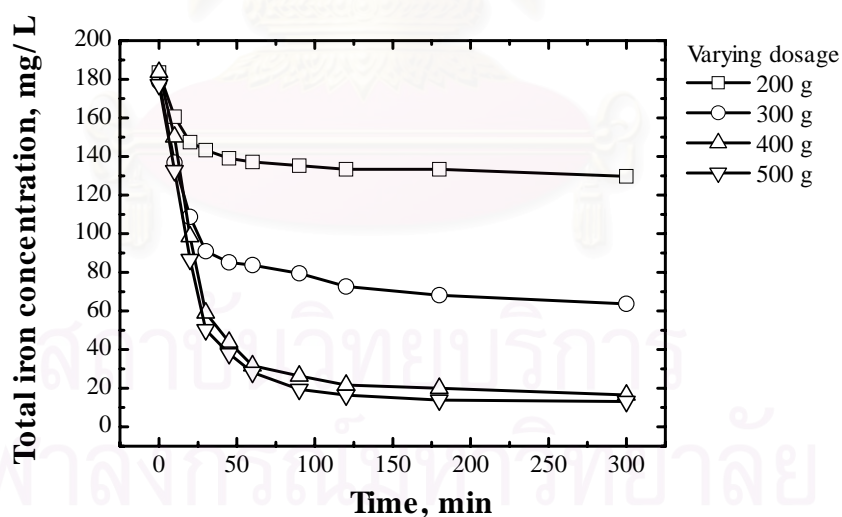


Figure 4.18 Effect of aluminum oxide dosage on the iron removal in fluidized bed process. (The initial iron concentration was 185 mg/L. The amount of sand dosage used in these experiments was varied from 200, 300, 400 and 500 g/L. The bed expansion was controlled at 0.5 from the original bed level. The initial pH was set at 6.5)

4.2 Iron Pellets Application for Copper Removal

4.2.1 Equilibrium Time

As copper ions can firmly adsorb onto the interface of iron pellets (F-ICS, T-ICS and T-ICAO). It is important to determine the time for copper adsorption onto iron coated carrier to reach equilibrium. A batch operation with 4 g of each adsorbent was used to remove copper at an initial concentration of 63.5 mg/L by controlled condition at pH 5.5 and 150 rpm for mixing intensity. Figure 4.19 showed the reaction of copper ions on iron coated sand which reaches to equilibrium in 2 hrs. Meanwhile, the total irons that leach from both kinds of media carrier were also analyzed. Figure 4.20 showed that F-ICS had larger amount of iron leach to solution than T-ICS, it was supported by results iron leaching test (topic 4.1.2) at pH 6.5. For three phase iron coated aluminum oxide was required 1.30 hrs to achieve the equilibrium (Figure 4.21).

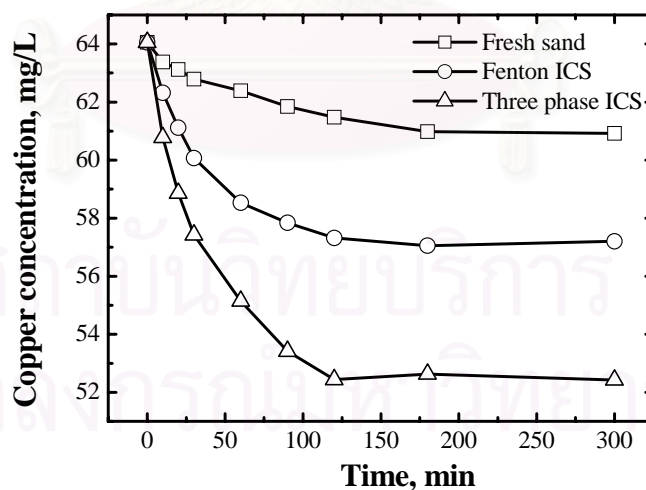


Figure 4.19 Equilibrium time of fresh sand, F-ICS and T-ICS for adsorption copper. (The initial copper was prepared at 63.5 mg/l. from copper nitrate (CuNO_3)₂. 4 g. of each type was used in experiment and pH was constant at 5.5 during the experiment. Adjust background ionic strength by 1 N. NaNO_3)

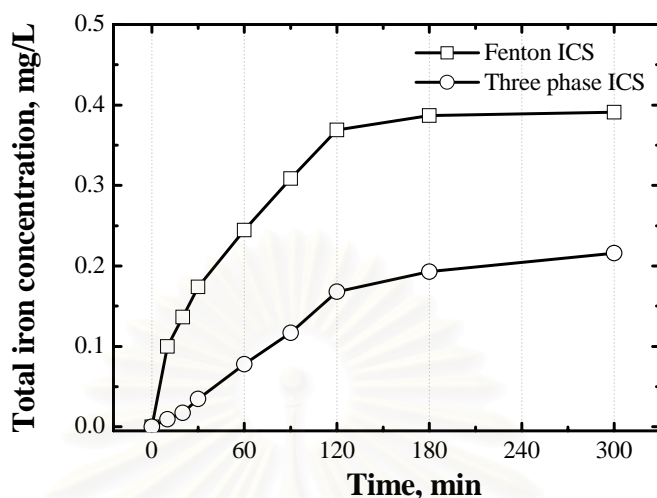


Figure 4.20 The iron leaching from media carrier as a function of time in adsorption process

4.2.2 Effect of pH on Copper Removal

To further understand the behavior of copper adsorption, the effect of pH on copper removal in adsorption process was studied at an initial pH of 5.5. Two scenarios were used, i.e., maintaining pH at 5.5 and without control. Figure 4.22 revealed that F-ICS could reduce copper ion to 57.20 and 47.98 mg/l at 3 hours in case of control and without control of pH, respectively. The final pH for without control strategy was 6.45. While copper ion was reduce by T-ICS (Figure4.23) to 52.42 mg/l for constant pH case and 48.16 mg/l for variable pH case with the final pH of 6.11. From both results, pH played an important role on copper removal; the greater removal of copper was obtained with increasing pH.

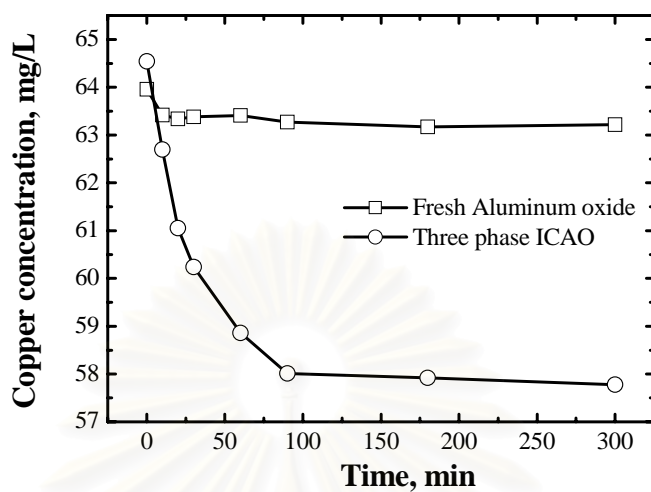


Figure 4.21 Equilibrium time of fresh Al_2O_3 and T-ICAO for adsorption copper. (The initial copper was prepared at 63.5 mg/l. from copper nitrate (CuNO_3)₂ 4 g. of each type was used in experiment and pH was constant at 5.5 during the experiment. Adjust background ionic strength by 1 N. NaNO_3)

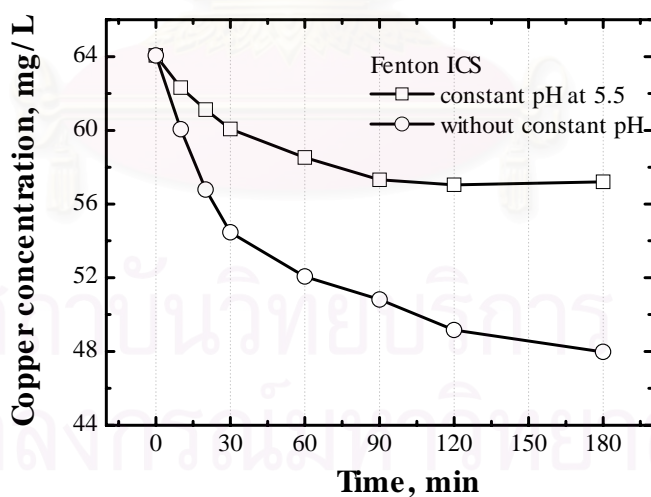


Figure 4.22 Effect of pH increasing on copper removal by F-ICS. (The initial copper was prepared at 63.5 mg/l. from copper nitrate (CuNO_3)₂ 4 g. of F-ICS was used in experiment. Adjust background ionic strength to 1 N. NaNO_3)

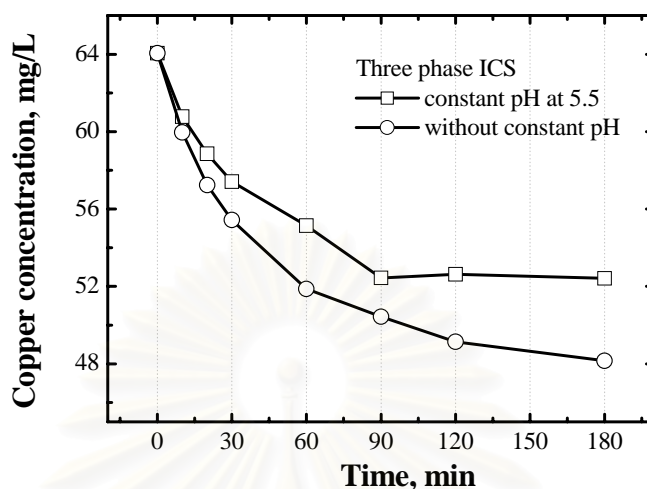


Figure 4.23 Effect of pH increasing on copper removal by T-ICS. (The initial copper was 63.5 mg/l, 4 g. of T-ICS was used in experiment. Adjust background ionic strength to 1 N. NaNO_3)

Due to increased hydroxyl groups were thought to increase the number of negative charged size enlarged the attraction force between metals ion and iron coated sand surface. Therefore, increasing the amount of copper ion adsorbed on iron coated sand surface (Lai, C.H., and Chen, C.Y, 2000). In addition, the precipitation of copper can be expected as well at pH 6. Therefore, It is also possible that some of copper was precipitated out in a form of $\text{Cu}(\text{OH})_3$ which is beneficial for real plant operation.

4.2.3 Adsorption Isotherm

In order to characterize the adsorption of copper on iron pellets, the adsorption isotherm was determined. The initial copper was prepared at 63.5 mg/l. from copper nitrate (CuNO_3)₂. The dosages for each type of iron pellets were at 1, 2, 4, and 8 g and pH was constant at 5.5. Adjust background ionic strength to 1 N. NaNO_3 . The isotherms of copper ion on F-ICS, T-ICS and T-ICAO were shown in

Figures 4.25, 4.26 and 4.27. While Langmuir plateau adsorption was observed between copper and iron pellets had better than Freundlich adsorption as illustrated in Table 4.6. The sorption coefficient (K_L) on iron pellets were 9.16×10^{-3} , 17.73×10^{-3} and 9.68×10^{-3} L/g for F-ICS T-ICS and T-ICAO, respectively. In term of maximum adsorption capacity (A_m) were achieved at 0.249, 0.300 and 0.222 mg Cu/g of pellets for F-ICS, T-ICS and T-ICAO, respectively.

Regarding to Langmuir adsorption isotherm of copper ion adsorbed on each type of iron pellets, equations 4.4, 4.5 and 4.6 reported linear equation which is a plot of one per adsorption quantity ($1/q$) against one per aqueous equilibrium concentration of copper ($1/C_e$) for F-ICS, T-ICS and T-ICAO respectively.

$$y = 438.65 x + 4.0223 \quad (4.4)$$

$$y = 188.05 x + 3.3326 \quad (4.5)$$

$$y = 465.54 x + 4.5035 \quad (4.6)$$

There are two roles to provide a copper adsorbed on media carrier, first amount of iron oxide that coated on each media and another one is the iron oxide species. Base on results from iron pellets preparation part (topic 4.1), the amount of iron oxide on their surface was slightly different. However, F-ICS was less stable than T-ICS at pH 5.5 that is a reason why T-ICS was obtained higher maximum adsorption capacity. Moreover, the iron oxide species play an important role on copper removal, the results indicated that T-ICS was belong to the kinds of goethite, $FeO(OH)$ which an excellent species for heavy metals removal (Grimme, 1968; Hildebrand and Blum, 1974; Mckenzie 1983; Gerth and Brümmer 1983). Therefore, T-ICS was achieved a highest maximum adsorption capacity and followed by F-ICS and T-ICAO which non significant differently.

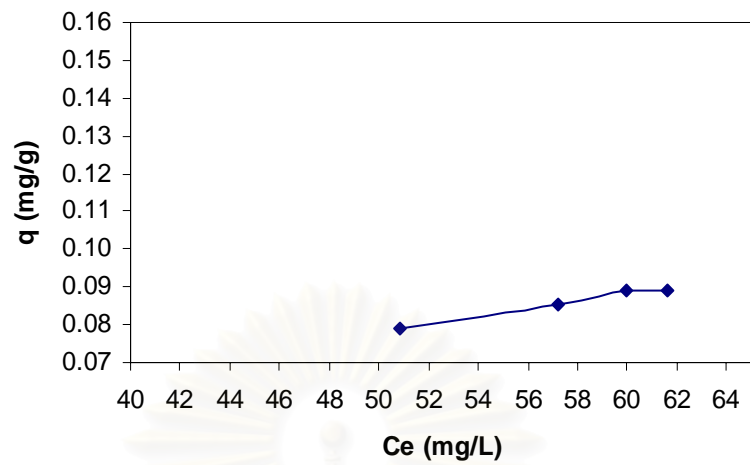


Figure 4.24 The isotherm of copper ion on F-ICS.

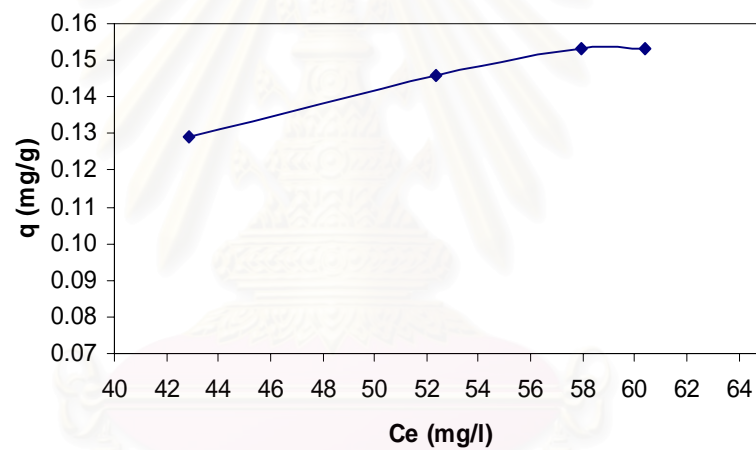


Figure 4.25 The isotherm of copper ion on T-ICS.

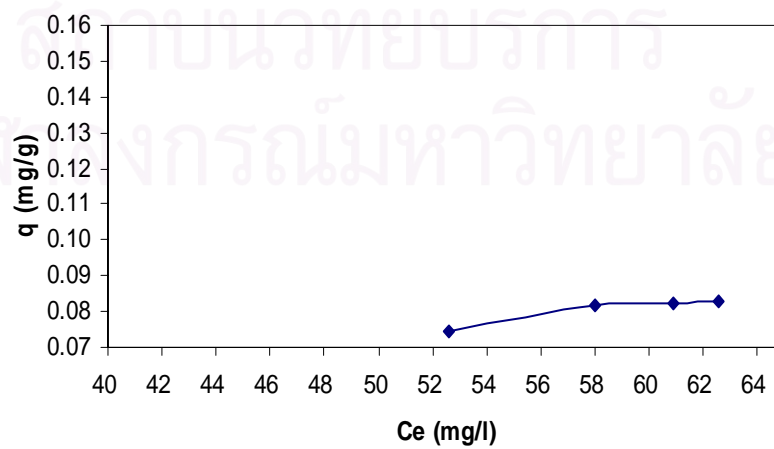


Figure 4.26 The isotherm of copper ion on T-ICAO.

Table 4.6 Summary of the adsorption isotherm by Langmuir and Freundlich isotherm of copper ion on different types of iron pellets.

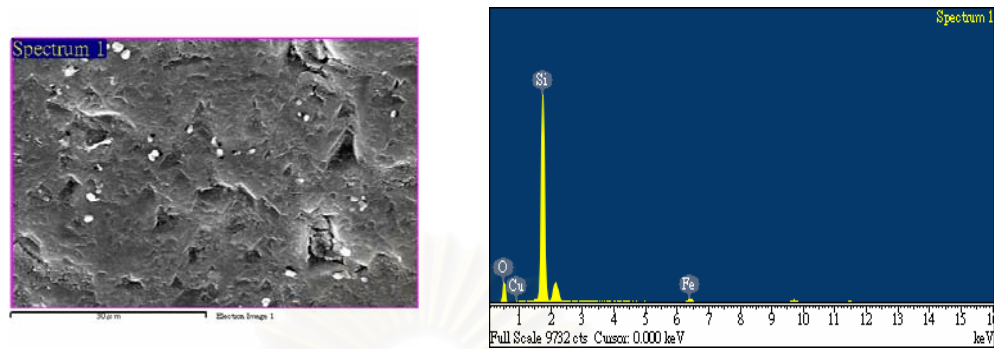
Type of iron pellets	Langmuir isotherm			Freundlich isotherm		
	Am mg Cu/g	K _L l/mg Cu	R ²	n	K _f	R ²
F-ICS	0.249	9.16 x 10 ⁻³	0.986	1.52	5.92 x 10 ⁻³	0.984
T-ICS	0.300	17.73 x 10 ⁻³	0.985	1.92	18.24 x 10 ⁻³	0.977
T-ICAO	0.222	9.68 x 10 ⁻³	0.912	1.58	6.08 x 10 ⁻³	0.903

4.2.4 Surface Characterization of Iron Pellets after Copper Adsorption

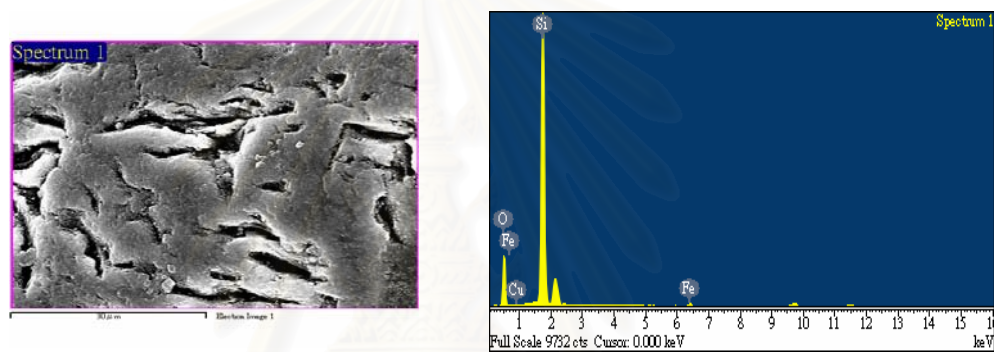
After copper adsorption, the solid sample was examined for surface characterization by using SEM/EDS. Figure 4.28(a), (b) and (c) showed EDS spectrum for the copper adsorption system which suggested that copper became one of the principle elements on the surface of solid sample. This was due to the fact that copper ions were chemisorbed on the surface of iron pellets. EDS analysis therefore provides a direct evidence for specific adsorption of copper ions on the surface of iron coated media. These results are in agreement with those previously reports of several researchers (Lo et al. (1997), Lo and Chen (1997), Lai and Chen (2000)) who revealed that chromate were chemisorbed onto the iron oxide surface.

In addition, surface composition of each kind of iron pellets was also investigated. The results in Table 4.7 express the weight percentage of each element including copper that attached on the surface. Therefore, it implied that copper ion indeed adsorbed onto iron pellets surface.

(a)



(b)



(c)

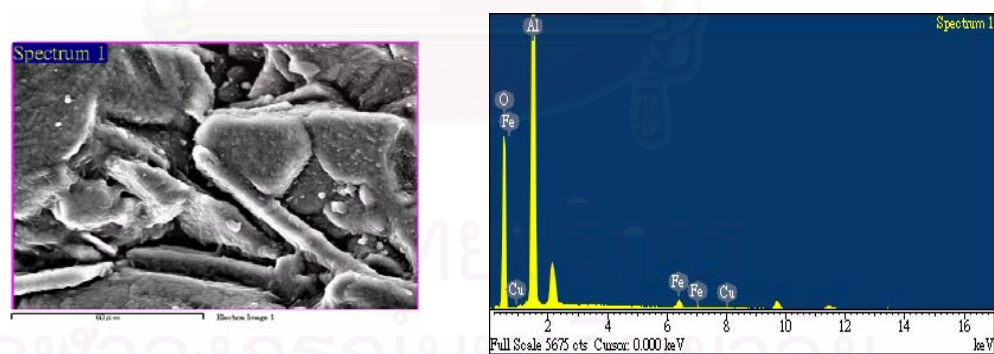


Figure 4.27 Surface morphology and EDS spectrum comparisons of iron pellets after copper adsorption by SEM and EDS: (a) F-ICS (b) T-ICS; (c) T-ICAO.

Table 4.7 Surface composition of F-ICS, T-ICS and T-ICAO after copper adsorption by SEM-EDS.

	Fe	Si	Al	O	Cu	Total
Element	%	%	%	%	%	%
	Weight	Weight	Weight	Weight	Weight	Weight
F-ICS	1.38	50.08	-	48.09	0.44	100
T-ICS	3.55	58.12	-	37.49	0.85	100
T-ICAO	0.98	-	49.06	49.41	0.54	100

4.2.5 Managerial Prospect

As all objectives have been fulfilled, iron coating technique has been optimized in both physical and chemical conditions and carrier materials. The findings from this study can be applied in field practice to lessen the disadvantages deriving from the applications of zero-valent iron and Fenton's family technologies. In term of managerial prospects, this iron coating technique can eliminate the requirement of sludge dewatering facility as well as reduce the disposed sludge volume. Considering based on their moisture contents, the moisture in iron-coated media almost approaches zero whereas that of dewatered iron hydroxide sludge is typically around 75%. Hence, with similar iron mass, the disposal weight of iron-coated media will be approximately only one-quarter of dewatered iron hydroxide sludge. As a result, the disposal cost can be reduced substantially in an expense of addition media. Additionally, these iron coated carriers can also be reutilized as an alternative material for heavy metal sorption; hence, reducing the treatment cost.

CHAPTER V

CONCLUSIONS AND RECOMMENDATIONS

5.1 Conclusions

The techniques to remove Fe^{2+} produced from Fe^0/CO_2 process were studied thoroughly. Two methods for ferrous oxidation to ferric, i.e., Fenton pretreatment and in-situ aeration transformation, were employed prior to iron pelletization onto fluidized-bed media. Two types of seeding materials, i.e., sand (SiO_2) and aluminum oxide (Al_2O_3), were focused although sand was used more intensively. Under the studied conditions for Fenton pretreatment, optimal pH, bed expansion, and sand dosage for iron removal were 6.5, 0.5, and 400 g/L, respectively, which could remove up to 98% of 185 mg/L of total iron being added within 2 hours. Specific and availability of surface area of sand seem to play an important role for iron coating. As a result, the reusability of iron-coated sand was somehow limited, i.e., iron removal efficiency gradually reduced from 98% in the first batch to 37% in the 11th batch with the specific coating capacity of 3.56 mg/g sand and specific coating surface of 25.75%. Iron coating specie was found to be $\text{Fe}(\text{OH})_3$.

For in-situ aeration transformation using a three-phase fluidized bed reactor, the optimum air flow rate and sand dosage were achieved at 20mL/min and 400 g/L, respectively, which provided specific coating capacity of 0.431 mg/g sand, specific coating surface of 1.90% at the first batch operation. The $\text{FeO}(\text{OH})$ was identified as a major iron specie attached onto the sand surface. In term of iron-leaching resistibility, three-phase iron coated sand was more stable at wider pH range (5-9) than Fenton pretreated iron coated sand (only pH of 7).

For three-phase iron coated aluminum oxide, the optimum conditions were attained at pH 6.5 and 400 g/L of media which provided a specific capacity of 0.417 mg/g, and a specific coating surface of 1.01%. In addition, the coating specie was found to be mainly Fe₂O₃.

Iron-coated sands were found to be able to adsorb copper and the adsorption isotherms were better fitted by Langmuir isotherm. The maximum adsorption capacity and the Langmuir coefficient of Fenton pretreated iron coated sand were 0.249 mg Cu/g and 9.16×10^{-3} L/mg, respectively. For three-phase iron coated sand, the maximum adsorption capacity was 0.300 mg Cu/g and the Langmuir coefficient was 17.73×10^{-3} L/mg. For three-phase iron coated aluminum oxide, the maximum adsorption capacity and the Langmuir coefficient were 0.222 mg Cu/g and 9.68×10^{-3} L/mg, respectively.

5.2 Recommendation

The results of this study provided valuable information of different iron coating process. However, iron pelletization process should have further study for improving their coating efficiency. A continuously operation, rather than a batch mode as in this study, might provide a better pelletization rate. Other cationic ions other than copper should be tested to provide more information for field practice.

REFERENCES

- Alowitz, M.J., and Scherer, M.M. Kinetics of nitrate, nitrite, and Cr(VI) reduction by iron metal. Environmental Science and Technology, 36 (2002): 299-306.
- Barrow, N.J., Bowden, J.W., Posner, A.M., and Quirk, J.P. Describing the adsorption of copper, zinc, and lead on a variable charge mineral surface. Aust. J. Soil Res., 19 (1981): 309-321.
- Borggaard, O.K. Effect of surface area and mineralogy of iron oxides on their surface charge and anion-adsorption properties. Clays Clay Miner, 31 (1983): 230-232.
- Bowden, J.W., Posner, A.M., and Quirk, J.P. Ionic adsorption on variable charge mineral surfaces: Theoretical charge development and titration curves. Aust J. Soil Res., 18 (1977): 49-60.
- Bowden, J.W., Nagarajah, S., Barrow, N.J., Posner, A.M., and Quirk, J.P. Describing the adsorption of phosphate, citrate, and selenite on a variable charge minerals surface. Aust. J. Soil Res., 18 (1980): 49-60.
- Breeuwsma A. Adsorption of ions on hematite (α -Fe₂O₃). Wageningen: Med. Landbouwhogehoe school, 1973.
- Brümmer, G.W., Gerth, J., and Tiller, K.G. Reaction kinetics of the adsorption and desorption of nickel, zinc, and cadmium by goethite. I. Adsorption and diffusion of metals. J. Soil Sci., 39 (1988): 37-52.
- Chen, H.Y., Yeh, H.H., Tsai, M.C., and Lai, W.L. The application of fluidized bed crystallization in drinking water softening. Journal of the Chinese Institute of Environmental Engineering 10 (2000): 177-184.

- Cheng, S.F., and Wu, S. C. The enhancement methods for the degradation of TCE by zero valent metals. Chemosphere, 41 (2000): 1263–1270.
- Davidson, J.F., Clift, R., Harrison, D. Fluidization. 2 nd ed. Orlando: Academic Press, 1985.
- Deng, Y.W. Formation of iron (III) hydroxides from homogeneous solutions. Wat. Res. 31, 6 (1997): 1347-1354.
- Deutsch, W.J. Groundwater Geochemistry : Fundamentals and Applications to Contamination. Florida : Lewis Publishers, 1997.
- Eckenfelder, W. Industrial Pollution Control. 3 rd ed. Singapore:McGraw-Hill Book Co, 2000.
- Forbes, E.A., Posner, A.M., and Quirk, J.P. The specific adsorption of divalent Cd, Co, Pb, and Zn on goethite. J. Soil Sci., 27 (1976): 154-166.
- Gast, R.G., Landa, E.R., and Meyer, G.W. The interaction of water with goethite (α -FeOOH) and amorphous hydrated ferric oxide surfaces. Clays Clay Miner, 22 (1974): 31-39.
- Gerth, J., and Brümmer, G. Adsorption und Festlegung von Nickel, Zink, und Cadmium durch Goethit (α -FeOOH), Fresenius' Z. Anal. Chem., 316 (1983): 616-620.
- Grimme, H. Die adsorption von Mn, Co, Cu, und Zn durch Goethit aus verdünnten Lösungen. Z. Pflanzenernähr. Bodenk, 121 (1968): 58-65.
- Hilderbrand, E.S., and Blum, W.E. Lead fixation by iron oxides. Naturwissenschaften, 61 (1974): 169-170.
- Hingston, F.J., Atkinson, R.J., Posner, A.M., and Quirk, J.P. Specific adsorption of anions on goethite. Trans. Int. Congr. Soil Sci., 1 (1968): 669-678.

- Hlavay, J.S., and Polyák, K.R. Determination of surface properties of iron hydroxide-coated alumina adsorbent prepared for removal of arsenic from drinking water. Journal of Colloid and Interface Science, 284 (2004): 71–77.
- Hsu, C.Y., Liao, C.H., and Lu, M.C. Treatment of aqueous nitrate by zero valent iron powder in the presence of CO₂ bubbling. Groundwater Monitoring and Remediation, 24 (2004): 82-87.
- Kanel, S.R., Manning, B., Charlet, L., and Choi, H. Removal of Arsenic(III) from Groundwater by Nanoscale Zero-Valent Iron. Environ. Sci. Technol., 39 (2005): 1291-1298.
- Kim, Y.H., and Carraway, E.R. Dechlorination of pentachlorophenol by zerovalent iron and modified zero valent irons. Environ. Sci. Technol., 34 (2000): 2014–2017.
- Lai, C.H., Lo, S.L., and Chiang, H.L. Adsorption/desorption properties of copper ions on the surface of iron-coated sand using BET and EDAX analyses, Journal of Chemosphere (1999): 1249-1255.
- Lai, C.H., and Chen, C.Y. Removal of metal ions and humic acid from water by iron-coated filter media. Chemosphere, 44 (2000): 1177-1184.
- Le, Z. A method for preparing silica-containing iron(III) oxide adsorbents for arsenic removal. Journal of water research, 37 (2003): 4351-4358.
- Lee, C.I., Yang, W.F., Hsieh, C.I. Removal of copper (II) by manganese-coated sand in a liquid fluidized-bed reactor. Journal of Hazardous Materials, B114 (2004): 45–51.

- Liao, C.H., Kang, S.F., and Hsu, Y.W. Zero-valent iron reduction of nitrate in the presence of ultraviolet light, organic matter and hydrogen peroxide. Water Research, 37 (2003): 4109-4118.
- Lin, C.J., and Chang, J.E. Effect of fly ash characteristics on the removal of Cu (II) from aqueous solution. Chemosphere, 44 (2000): 1185-1192.
- Lo, S.L., and Chen, T.Y. Adsorption of Se (IV) and Se (VI) on an iron coated sand from water. Journal of Chemosphere (1997): 919-930.
- Lo, S.L., Jeng, H.T., and Lai, C.H. Characteristic and adsorption properties of iron coated-sand. Wat.Sci. Tech. (1997): 63-70.
- McKenzie, R.M. The adsorption of lead and other heavy metals on oxides of manganese and iron. Aust. J. Soil Res., 18 (1980): 61-73.
- McKenzie, R.M. The adsorption of molybdenum on oxide surfaces. Aust. J. Soil Res., 21 (1983): 505-513.
- Park, G.A., and Bruyn, P.L. The zero point of charge of oxides. J. Phys. Chem., 66 (1962): 967-973.
- Park, G.A. The isoelectric point of solid oxides, solid hydroxides, and aqueous hydroxy complex systems. Chem. Rev., 65 (1965): 177-198.
- Park, G.A. Aqueous surface chemistry of oxides and complex oxide minerals: Isoelectric point and zero point of charge. In R.F. Gould (ed.) Equilibrium concepts in natural water systems. Adv. Chem. Ser., 67 (1967): 121-160.
- Perry Robert, H. Chemical Engineer's Handbook. Mc Graw Hill.
- Pignatello, J.J. Dark and photoassisted Fe³⁺- catalyzed degradation of chlorophenoxy herbicides by hydrogen peroxide. Environ. Sci. Technol., 26 (1992): 944-951.

- Schulze, D.G., and Schwertmann, U. The influence of aluminium on iron oxides. X. The properties of Al substituted goethites. Clay Miner, 19 (1984): 521-529.
- Schwertmann, U., and Fechter, H. The point of zero charge of natural and synthetic ferrihydrites and its relation to adsorbed silicate. Clay Miner, 17 (1982): 471-476.
- Schwertmann, U., Cambier, P., and Murad, E. Properties of goethites of varying crystallinity. Clays Clay Miner, 33 (1985): 369-378.
- Snoeyink, V., and Jenkins, D. Water Chemistry: Inc. Standard Methods for the Examination of Water and Wastewater. 19th ed (1995). Washington DC: American Public Health Association/American Water Works Association/Water Environment Federation, 1980.
- Tessens, E., and Zauyah, S. Positive permanent charge in oxisols. Soil Sci. Soc. Am. J., 46 (1982): 1103-1106.
- Van Der Veen, C., and Graveland, A. Central softening by crystallization in a fluidized bed process. Journal AWWA (1988): 51-56.
- Wann, S.S., and Uehara, G. Surface charge manipulation in constant surface potential soil colloids. II. Effect on solute transport. Soil Sci. Soc. Am. J., 42 (1978): 886-888.
- Xu, Y., and Axe, L. Synthesis and characterization of iron oxide-coated silica and its effect on metal adsorption. Journal of Colloid and Interface Science, 282 (2004): 11-19.
- Yaron, B., Calvert, R., and Prost, R. Soil Pollution : Processes and Dynamics. Germany: Springer-Verlag Berlin Heidelberg, 1996.

Zhou, P., Huang, J.C., Li, A.W.F., and Wei, S. Heavy metal removal from wastewater in fluidized bed reactor. Water Research, 33 (1999): 1918-1924.



สถาบันวิทยบริการ
จุฬาลงกรณ์มหาวิทยาลัย



สถาบันวิทยบริการ
จุฬาลงกรณ์มหาวิทยาลัย

A. Fenton Pretreatment Fluidized bed process (ICS)

Table A1 Effect of Initial pH on Iron Coating onto Sand Surface in Fluidized Bed Process (pH of 4.40)

Time (min)	pH	Total iron (mg/L)
0	4.37	190.50
10	4.46	186.70
20	4.55	180.94
30	4.62	175.50
45	4.68	171.62
60	4.72	165.54
90	4.76	154.50
120	4.78	135.70
180	4.82	125.50
300	4.87	120.44

Table A2 Effect of Initial pH on Iron Coating onto Sand Surface in Fluidized Bed Process (pH of 6.50)

Time (min)	pH	Total iron (mg/L)
0	6.55	180.60
10	6.58	158.90
20	6.6	144.47
30	6.61	123.40
45	6.60	102.50
60	6.62	86.50
90	6.63	55.50
120	6.64	36.40
180	6.65	15.75
300	6.68	7.23

Table A3 Effect of Initial pH on Iron Coating onto Sand Surface in Fluidized Bed Process (pH of 12.00)

Time (min)	pH	Total iron (mg/L)
0	12.00	185.80
10	11.58	182.60
20	12.00	183.20
30	12.00	181.00
45	12.00	179.60
60	12.00	175.60
90	12.00	173.40
120	12.00	173.20
180	12.00	172.80
300	12.00	171.60

Table A4 Effect of Recirculation Flow Rate on Iron Coating onto Sand surface in Fluidized Bed Process (0.50 bed expand, 2100 ml/min)

Time (min)	pH	Total iron (mg/L)
0	6.55	180.60
10	6.58	158.90
20	6.60	144.47
30	6.61	123.40
45	6.60	102.50
60	6.62	86.50
90	6.63	55.50
120	6.64	36.40
180	6.65	15.75
300	6.68	7.23

Table A5 Effect of Recirculation Flow Rate on Iron Coating onto Sand surface in Fluidized Bed Process (0.75 bed expand, 2700 ml/min)

Time (min)	pH	Total iron (mg/L)
0	6.50	184.40
10	6.48	178.80
20	6.52	165.40
30	6.63	159.40
45	6.60	148.80
60	6.65	135.80
90	6.63	111.20
120	6.66	77.00
180	6.72	33.80
300	6.75	17.37

Table A6 Effect of Recirculation Flow Rate on Iron Coating onto Sand surface in Fluidized Bed Process (1.00 bed expand, 3300 ml/min)

Time (min)	pH	Total iron (mg/L)
0	6.51	193.50
10	6.54	183.60
20	6.55	176.50
30	6.52	169.62
45	6.56	163.02
60	6.60	152.90
90	6.61	136.84
120	6.66	117.70
180	6.74	77.22
300	6.78	37.40

Table A7 Effect of Sand Dosage on Iron Coating onto Sand Surface in Fluidized Bed Process (200 g/L)

Time (min)	pH	Total iron (mg/L)
0	6.50	178.82
10	6.50	170.20
20	6.49	159.60
30	6.49	150.60
45	6.50	135.00
60	6.50	121.45
90	6.51	87.93
120	6.52	65.54
180	6.55	39.16
300	6.62	26.20

Table A8 Effect of Sand Dosage on Iron Coating onto Sand Surface in Fluidized Bed Process (300 g/L)

Time (min)	pH	Total iron (mg/L)
0	6.55	180.60
10	6.58	158.90
20	6.60	144.47
30	6.61	123.40
45	6.60	102.50
60	6.62	86.50
90	6.63	55.50
120	6.64	36.40
180	6.65	15.75
300	6.68	7.23

Table A9 Effect of Sand Dosage on Iron Coating onto Sand Surface in Fluidized Bed Process (400 g/L)

Time (min)	pH	Total iron (mg/L)
0	6.52	188.58
10	6.48	142.74
20	6.51	120.50
30	6.58	85.44
45	6.60	60.56
60	6.60	35.52
90	6.64	12.38
120	6.67	9.12
180	6.73	6.06
300	6.93	3.27

Table A10 Effect of Sand Dosage on Iron Coating onto Sand Surface in Fluidized Bed Process (500 g/L)

Time (min)	pH	Total iron (mg/L)
0	6.56	183.67
10	6.59	139.40
20	6.62	101.31
30	6.63	72.50
45	6.65	49.20
60	6.60	23.80
90	6.68	9.70
120	6.69	6.50
180	6.70	4.25
300	6.72	1.88

Table A11 Effect of Ferric Concentration on Iron Coating onto Sand in Fluidized Bed Process (126 mg/L)

Time (min)	pH	Total iron (mg/L)
0	4.50	126.34
10	6.48	77.17
20	6.48	41.98
30	6.52	28.52
45	6.52	13.72
60	6.50	8.47
90	6.50	4.74
120	6.50	4.12
180	6.70	3.17
300	6.78	2.53

Table A12 Effect of Ferric Concentration on Iron Coating onto Sand in Fluidized Bed Process (188 mg/L)

Time (min)	pH	Total iron (mg/L)
0	6.52	188.58
10	6.48	142.74
20	6.51	120.50
30	6.58	85.44
45	6.60	60.56
60	6.60	35.52
90	6.64	12.38
120	6.67	9.12
180	6.73	6.06
300	6.93	3.27

Table A13 Effect of Ferric Concentration on Iron Coating onto Sand in Fluidized Bed Process (252 mg/L)

Time (min)	pH	Total iron (mg/L)
0	4.80	252.83
10	6.60	230.04
20	6.57	204.99
30	6.56	190.06
45	6.54	171.63
60	6.60	154.20
90	6.60	128.28
120	6.60	112.12
180	6.64	83.96
300	6.75	54.19

Table A14 Effect of Ferric Concentration on Iron Coating onto Sand in Fluidized Bed Process (334 mg/L)

Time (min)	pH	Total iron (mg/L)
0	4.75	334.24
10	6.50	309.29
20	6.55	285.77
30	6.51	268.19
45	6.52	243.23
60	6.53	221.88
90	6.53	188.33
120	6.55	161.11
180	6.60	124.61
300	6.68	82.33

Table A15. Repeatability of Sand for Iron Removal (1st batch operation)

Time (min)	pH	Total iron (mg/L)
0	4.55	187.65
10	6.38	135.47
20	6.52	96.32
30	6.60	56.04
45	6.70	44.36
60	6.86	29.19
90	6.74	14.06
120	6.80	7.26
180	6.95	5.60
300	7.18	4.33

Table A16. Repeatability of Sand for Iron Removal (3rd batch operation)

Time (min)	pH	Total iron (mg/L)
0	4.47	171.85
10	6.50	129.69
20	6.51	101.79
30	6.58	78.72
45	6.60	56.74
60	6.60	41.43
90	6.64	29.50
120	6.67	17.35
180	6.73	14.25
300	6.93	12.70

Table A17. Repeatability of Sand for Iron Removal (5th batch operation)

Time (min)	pH	Total iron (mg/L)
0	4.53	188.649
10	6.54	167.30
20	6.55	151.12
30	6.58	129.49
45	6.60	96.61
60	6.59	66.17
90	6.61	45.49
120	6.65	38.57
180	6.89	35.19
300	6.95	34.35

Table A18. Repeatability of Sand for Iron Removal (7th batch operation)

Time (min)	pH	Total iron (mg/L)
0	5.70	176.79
10	6.54	158.98
20	6.53	139.22
30	6.51	122.78
45	6.56	96.78
60	6.73	70.08
90	6.74	53.48
120	6.94	52.14
180	6.82	51.15
300	7.10	51.13

Table A19. Repeatability of Sand for Iron Removal (9th batch operation)

Time (min)	pH	Total iron (mg/L)
0	4.50	184.08
10	6.60	158.34
20	6.60	123.36
30	6.60	110.78
45	6.57	90.80
60	6.58	82.4
90	6.58	77.98
120	6.58	72.92
180	6.60	67.96
300	6.81	65.14

Table A20. Repeatability of Sand for Iron Removal (11th batch operation)

Time (min)	pH	Total iron (mg/L)
0	4.35	172.48
10	6.49	155.74
20	6.47	140.32
30	6.48	132.08
45	6.48	126.96
60	6.50	124.20
90	6.50	120.72
120	6.51	115.98
180	6.58	110.20
300	6.70	105.42

B. Graphics determination of first order rated constant analysis.

Figure B1-B4. Graphics determination of different sand dosage

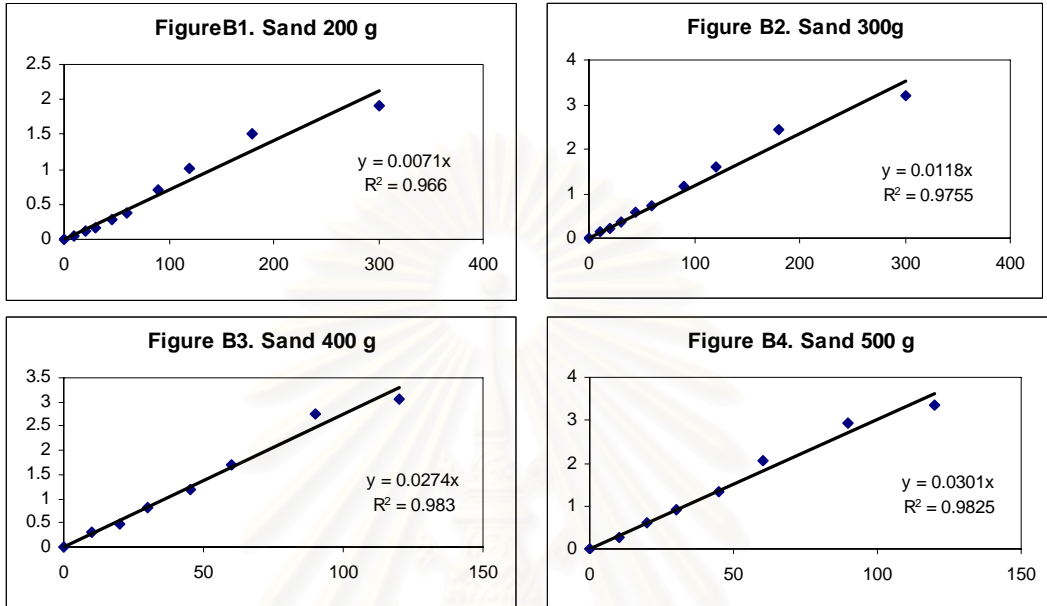
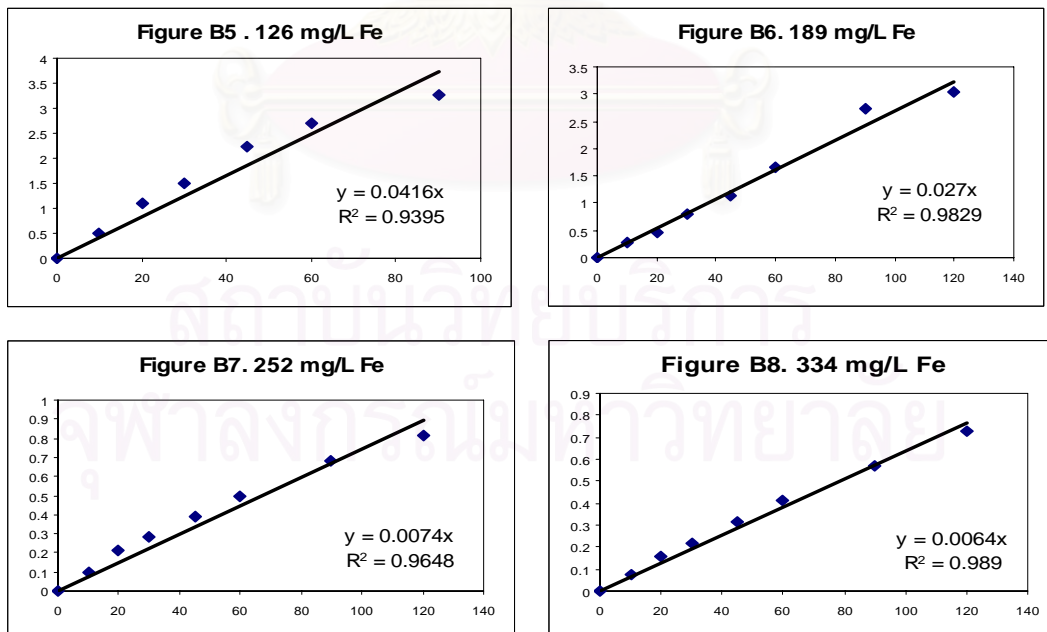


Figure B5-B8. Graphics determination of different initial iron concentration.



C. Three Phase Fluidized Bed Process (ICS)

Table C1. Effect of Air Flow Rate on Iron Coating onto Sand Surface in Three Phases Fluidized Bed Process. (20 ml/min)

Time (min)	pH	DO (mg/L)	ORP (MV)	Temp °C	Fe ²⁺ (mg/l)	Total iron (mg/L)
0	5.65	0.78	-204	31.3	189.04	189.74
10	5.82	1.66	-107	31.7	165.64	168.95
20	5.97	2.17	-111	32.3	135.03	144.29
30	6.21	3.73	-112	32.3	107.38	112.89
45	6.17	4.85	-78	32.5	69.63	73.54
60	6.29	4.87	-40	32.6	39.22	41.27
90	6.32	5.19	-12	32.6	9.36	24.10
120	6.43	5.82	58	32.7	0.00	15.29
180	6.54	7.26	164	32.8	-	11.21
300	6.78	7.38	250	33.1	-	9.57

Table C2. Effect of Air Flow Rate on Iron Coating onto Sand Surface in Three Phases Fluidized Bed Process. (100 ml/min)

Time (min)	pH	DO (mg/L)	ORP (MV)	Temp °C	Fe ²⁺ (mg/l)	Total iron (mg/L)
0	5.65	0.86	-191	31.8	187.09	188.14
10	5.78	0.28	-167	31.9	158.80	153.63
20	6.10	4.51	-91	32.1	100.04	126.40
30	6.26	4.68	-63	32.1	76.29	104.52
45	6.32	5.45	-48	32.2	47.12	72.56
60	6.48	7.09	2	32.5	23.98	47.77
90	6.65	6.67	57	32.3	0.000	32.35
120	6.76	7.32	86	31.9	-	23.58
180	6.82	7.80	112	32.1	-	19.28
300	7.02	7.86	152	32.3	-	17.10

Table C3. Effect of Air Flow Rate on Iron Coating onto Sand Surface in Three phases Fluidized Bed Process. (300 ml/min)

Time (min)	pH	DO (mg/L)	ORP (MV)	Temp °C	Fe ²⁺ (mg/l)	Total iron (mg/L)
0	5.61	0.88	-120	31.3	182.15	184.82
10	5.79	2.20	-106	31.7	133.14	142.54
20	6.12	3.05	-93	32.3	92.50	118.72
30	6.32	4.81	-72	32.3	51.23	94.28
45	6.58	6.89	-55	32.5	25.82	64.21
60	6.62	7.02	-27	32.5	14.56	49.79
90	6.71	7.80	-4	32.6	0.000	38.32
120	6.62	7.75	54	32.7	-	31.69
180	6.95	7.58	102	32.5	-	25.78
300	7.11	7.42	134	32.3	-	22.33

Table C4. Effect of Air Flow Rate on Iron Coating onto Sand Surface in Three Phases Fluidized Bed Process. (500 ml/min)

Time (min)	pH	DO (mg/L)	ORP (MV)	Temp °C	Fe ²⁺ (mg/l)	Total iron (mg/L)
0	5.41	0.61	-133	30.2	182.15	177.74
10	5.86	4.82	-63	30.6	110.15	132.54
20	6.09	6.73	-19	31.3	76.88	102.56
30	6.27	7.58	2	31.0	11.88	84.82
45	6.42	7.64	100	31.6	0.00	64.66
60	6.64	7.62	203	31.5	-	56.12
90	6.90	7.95	218	31.6	-	45.74
120	7.02	7.82	230	31.8	-	41.26
180	7.12	8.02	246	32.4	-	35.92
300	7.14	7.81	258	32.2	-	33.02

Table C5. Effect of Sand Dosage on Iron Coating onto Sand Surface in Three Phases Fluidized Bed (200 g/L)

Time (min)	pH	DO (mg/L)	ORP (MV)	Temp °C	Fe ²⁺ (mg/l)	Total iron (mg/L)
0	5.84	0.91	-156	30.2	185.62	182.8
10	5.62	1.59	-134	30.1	155.14	173.6
20	5.87	3.57	-113	30.2	132.75	161.4
30	5.99	3.92	-84	31.3	113.67	157.3
45	6.22	5.69	-66	31.5	86.24	135.6
60	6.14	6.35	-18	31.7	53.04	119.7
90	6.39	6.75	28	31.4	23.18	89.1
120	6.33	6.88	76	32.0	4.22	66.7
180	6.55	7.18	134	32.1	-	44.6
300	6.81	7.01	186	32.5	-	30.2

Table C6. Effect of Sand Dosage on Iron Coating onto Sand Surface in Three Phases Fluidized Bed (300 g/L)

Time (min)	pH	DO (mg/L)	ORP (MV)	Temp °C	Fe ²⁺ (mg/l)	Total iron (mg/L)
0	5.65	0.94	-121	31.5	179.55	192.1
10	5.78	1.39	-112	31.7	157.51	172.6
20	5.90	3.13	-101	32.2	124.59	150.2
30	5.83	4.57	-96	32.3	98.49	138.6
45	6.12	5.43	-83	32.6	67.23	110.7
60	6.25	5.64	-53	32.7	40.21	88.6
90	6.30	6.48	20	32.9	12.78	52.2
120	6.32	6.96	58	33.0	0.00	32.8
180	6.48	6.18	104	32.9	-	20.0
300	6.67	6.98	200	32.1	-	15.6

Table C7. Effect of Sand Dosage on Iron Coating onto Sand Surface in Three Phases Fluidized Bed (400 g/L)

Time (min)	pH	DO (mg/L)	ORP (MV)	Temp °C	Fe ²⁺ (mg/l)	Total iron (mg/L)
0	5.65	0.78	-204	31.3	189.04	189.74
10	5.82	1.66	-107	31.7	165.64	168.95
20	5.97	2.17	-111	32.3	135.03	144.29
30	6.21	3.73	-112	32.3	107.38	112.89
45	6.17	4.85	-78	32.5	69.63	73.54
60	6.29	4.87	-40	32.6	39.22	41.27
90	6.32	5.19	-12	32.6	9.36	24.10
120	6.43	5.82	58	32.7	0.00	15.29
180	6.54	7.26	164	32.8	-	11.21
300	6.78	7.38	250	33.1	-	9.57

Table C8. Effect of Sand Dosage on Iron Coating onto Sand Surface in Three Phases Fluidized Bed (500 g/L)

Time (min)	pH	DO (mg/L)	ORP (MV)	Temp °C	Fe ²⁺ (mg/l)	Total iron (mg/L)
0	5.72	1.02	-126	31.1	176.50	185.4
10	5.93	1.98	-91	31.3	150.17	145.6
20	5.81	2.36	-95	32.1	123.98	122.2
30	6.11	4.12	-102	31.3	96.83	89.4
45	6.09	5.67	-89	32.5	72.56	61.8
60	6.35	5.24	-78	32.2	33.62	29.4
90	6.44	6.35	-5	32.2	6.36	18.2
120	6.50	6.80	54	33.5	1.20	13.8
180	6.55	7.13	102	33.9	-	10.6
300	6.58	7.68	196	33.7	-	8.8

D. Three Phase Fluidized Bed Process (ICAO)

Table D1. Effect of Initial pH on the Iron Coating onto Aluminum Oxide Surface in Three Phase Fluidized Bed Process.(pH of 5.5)

Time (min)	pH	DO (mg/L)	ORP (MV)	Temp °C	Fe ²⁺ (mg/l)	Total iron (mg/L)
0	5.54	0.82	-100	32.2	190.44	186.58
10	5.78	1.31	-96	32.3	171.18	170.70
20	5.82	2.46	-92	33.3	155.28	157.04
30	5.83	2.68	-90	33.0	136.87	143.70
45	5.91	4.85	-86	33.4	113.71	114.10
60	5.88	5.45	-65	33.7	61.26	78.08
90	5.96	5.74	-22	32.8	18.85	47.88
120	6.02	5.66	11	32.3	0.00	37.94
180	6.29	6.30	71	32.9	-	35.60
300	6.56	7.02	156	32.2	-	35.84

Table D2. Effect of Initial pH on the Iron Coating onto Aluminum Oxide Surface in Three Phase Fluidized Bed Process.(pH of 6.5)

Time (min)	pH	DO (mg/L)	ORP (MV)	Temp °C	Fe ²⁺ (mg/l)	Total iron (mg/L)
0	6.52	1.26	-191	31.3	172.30	183.64
10	6.43	1.40	-167	31.7	158.63	150.08
20	6.32	2.20	-123	32.3	132.96	98.46
30	6.45	3.05	-91	32.3	83.30	58.96
45	6.58	2.22	-63	32.5	46.20	43.88
60	6.68	2.65	-48	32.5	29.73	31.64
90	6.75	4.81	-17	32.6	22.48	26.34
120	6.84	4.75	0	32.7	0.00	21.64
180	6.95	6.89	57	32.5	-	19.99
300	6.96	6.90	152	32.3	-	16.55

Table D3. Effect of Aluminum Oxide Dosage on Iron Coating onto Aluminum Oxide Surface in Three Phase Fluidized Bed Process (200 g/L)

Time (min)	pH	DO (mg/L)	ORP (MV)	Temp °C	Fe ²⁺ (mg/l)	Total iron (mg/L)
0	6.53	0.34	-165	31.2	165.33	183.48
10	6.32	2.25	-125	31.4	116.78	160.64
20	6.28	3.65	-96	31.5	86.93	147.44
30	6.29	3.13	-69	31.5	55.96	143.24
45	6.39	5.80	-32	31.5	32.25	139.08
60	6.30	6.77	-14	31.5	22.48	137.10
90	6.38	6.90	33	31.7	10.76	135.30
120	6.49	7.12	57	31.7	0.00	133.34
180	6.55	6.91	131	31.8	-	133.36
300	6.96	6.58	185	31.4	-	129.68

Table D4. Effect of Aluminum Oxide Dosage on Iron Coating onto Aluminum Oxide Surface in Three Phase Fluidized Bed Process (300 g/L)

Time (min)	pH	DO (mg/L)	ORP (MV)	Temp °C	Fe ²⁺ (mg/l)	Total iron (mg/L)
0	6.54	0.34	-182	30.7	172.02	178.78
10	6.30	3.48	-117	31.2	139.10	136.78
20	6.21	5.25	-83	32.1	88.05	108.68
30	6.19	6.28	-51	32.1	62.10	90.96
45	6.23	6.30	-30	32.1	32.52	85.20
60	6.18	6.69	-9	32.3	19.14	83.76
90	6.32	6.50	29	32.8	16.62	79.52
120	6.47	6.87	70	32.7	0.00	72.62
180	6.67	6.27	121	32.3	-	68.18
300	6.85	6.40	148	32.2	-	63.72

Table D5. Effect of Aluminum Oxide Dosage on Iron Coating onto Aluminum Oxide Surface in Three Phase Fluidized Bed Process (400 g/L)

Time (min)	pH	DO (mg/L)	ORP (MV)	Temp °C	Fe ²⁺ (mg/l)	Total iron (mg/L)
0	6.52	1.26	-191	31.3	172.30	183.64
10	6.43	1.40	-167	31.7	158.63	150.08
20	6.32	2.20	-123	32.3	132.96	98.46
30	6.45	3.05	-91	32.3	83.30	58.96
45	6.58	2.22	-63	32.5	46.20	43.88
60	6.68	2.65	-48	32.5	29.73	31.64
90	6.75	4.81	-17	32.6	22.48	26.34
120	6.84	4.75	0	32.7	0.00	21.64
180	6.95	6.89	57	32.5	-	19.99
300	6.96	6.90	152	32.3	-	16.55

Table D6. Effect of Aluminum Oxide Dosage on Iron Coating onto Aluminum Oxide Surface in Three Phase Fluidized Bed Process (500 g/L)

Time (min)	pH	DO (mg/L)	ORP (MV)	Temp °C	Fe ²⁺ (mg/l)	Total iron (mg/L)
0	6.46	0.42	-166	31.8	166.16	177.24
10	6.30	1.74	-132	31.9	120.68	132.72
20	6.20	1.99	-107	32.1	79.40	86.74
30	6.21	2.57	-87	32.1	42.85	50.22
45	6.26	4.12	-57	32.3	35.06	37.88
60	6.29	4.93	-42	32.5	23.04	28.15
90	6.38	6.72	2	32.5	0.79	19.36
120	6.54	7.31	47	31.9	0.00	16.37
180	6.62	7.08	126	32.1	-	13.80
300	6.84	7.10	156	32.3	-	13.07

E. Iron Pellets Leaching Test.

Table E1. Fenton Pretreated Iron Coated Sand leaching test at 72 hrs

Time (min)	Total iron (mg/L)				
	pH 3	pH 5	pH 7	pH 9	pH 12
0.00	0.0140	0.0093	0.0052	0.0211	0.0332
0.16	0.0501	0.0413	0.0114	0.0321	0.0831
0.50	0.0892	0.0821	0.0121	0.0445	0.1355
1.00	0.1116	0.0985	0.0217	0.0903	0.1705
1.50	0.1304	0.1186	0.0226	0.1281	0.1982
2.00	0.1520	0.1201	0.0239	0.1379	0.2297
3.00	0.1815	0.1254	0.0215	0.1581	0.2444
5.00	0.2349	0.1311	0.0233	0.1987	0.2641
10.00	0.2814	0.1632	0.0288	0.2503	0.3017
15.00	0.2833	0.1671	0.0214	0.2489	0.3115
24.00	0.2840	0.1745	0.0271	0.2493	0.3105
48.00	0.2885	0.1864	0.0272	0.2552	0.3108
72.00	0.2894	0.1831	0.0281	0.2602	0.3085

Table E2. Three Phase Iron Coated Sand leaching test at 72 hrs

Time (min)	Total iron (mg/L)				
	pH 3	pH 5	pH 7	pH 9	pH 12
0.00	0.0074	0.0047	0.0031	0.0103	0.0223
0.16	0.0416	0.0162	0.0048	0.0161	0.0642
0.50	0.0611	0.0152	0.0045	0.0126	0.1167
1.00	0.0826	0.0182	0.0053	0.0144	0.1496
1.50	0.0989	0.0191	0.0051	0.0152	0.1659
2.00	0.1026	0.0222	0.0067	0.0177	0.1751
3.00	0.1133	0.0275	0.0074	0.0195	0.1937
5.00	0.1262	0.0316	0.0097	0.0203	0.2258
10.00	0.1423	0.0439	0.0138	0.0244	0.2613
15.00	0.1412	0.0489	0.0118	0.0257	0.2650
24.00	0.1401	0.0497	0.0124	0.0266	0.2641
48.00	0.1447	0.0473	0.0126	0.0216	0.2635
72.00	0.1463	0.0486	0.0149	0.0246	0.2685

F. Iron Pellet Application for Copper Ion Removal.

Table F1. Equilibrium time of fresh sand

Time (min)	pH	Temp ⁰ C	Residuals Copper (mg/l)
0	5.50	30.0	64.06
5	5.48	31.1	63.92
10	5.51	31.0	63.78
20	5.49	32.0	63.61
30	5.50	30.0	63.59
45	5.42	31.0	63.52
60	5.45	31.0	63.48
90	5.47	31.0	63.41
120	5.48	31.0	63.32
180	5.40	31.0	63.35
300	5.44	30.0	63.42
600	5.51	30.0	63.37
900	5.51	31.0	63.35
1440	5.53	32.0	63.39

Table F2. Equilibrium time of Fenton Pretreated Iron Coated Sand

Time (min)	pH	Temp ⁰ C	Residuals Copper (mg/l)	Total iron (mg/L)
0	5.50	30.0	64.06	0.000
5	5.52	30.0	63.88	0.026
10	5.54	31.0	62.32	0.099
20	5.50	31.0	61.12	0.136
30	5.42	31.0	60.07	0.173
45	5.53	31.0	59.14	0.189
60	5.48	30.0	58.53	0.244
90	5.44	31.0	58.01	0.308
120	5.51	31.0	57.32	0.369
180	5.50	30.0	57.05	0.387
300	5.46	30.0	57.20	0.391
600	5.46	30.0	57.05	0.387
900	5.48	30.0	57.10	0.395
1440	5.51	31.0	57.06	0.380

Table F3. Equilibrium time of Three Phase Iron Coated Sand

Time (min)	pH	Temp °C	Residuals Copper (mg/l)	Total iron (mg/L)
0	5.49	30.0	64.06	0.000
5	5.51	30.0	62.88	0.000
10	5.50	30.0	60.78	0.009
20	5.50	31.0	58.86	0.017
30	5.51	30.0	57.42	0.035
45	5.50	30.0	56.34	0.021
60	5.52	30.0	55.14	0.078
90	5.48	30.0	53.69	0.117
120	5.50	30.0	52.44	0.168
180	5.45	30.0	52.63	0.193
300	5.51	31.0	52.42	0.216
600	5.50	31.0	52.36	0.203
900	5.51	30.0	52.41	0.216
1440	5.45	30.0	52.38	0.222

Table F4. Equilibrium time of Fresh Aluminum Oxide

Time (min)	pH	Temp °C	Residuals Copper (mg/l)
0	5.50	33.7	63.96
10	5.52	33.7	63.42
20	5.49	33.8	63.34
30	5.50	33.6	63.38
60	5.50	33.5	63.41
90	5.50	33.3	63.27
120	5.52	33.5	63.32
180	5.56	33.7	63.17
300	5.53	33.3	63.22
480	5.48	33.5	63.05
720	5.47	33.5	63.19

Table F5. Equilibrium time of Three Phase Iron Coated Aluminum Oxide

Time (min)	pH	Temp °C	Residuals Copper (mg/l)
0	5.50	32.3	64.54
10	5.48	32.6	62.70
20	5.54	32.7	61.05
30	5.56	32.8	60.24
60	5.49	32.3	58.86
90	5.55	32.4	58.12
120	5.48	32.8	58.01
180	5.50	32.3	57.92
300	5.51	32.3	57.78
480	5.53	32.3	57.59
720	5.50	32.3	57.71

Table F6. Effect of pH increasing on Copper Removal (F-ICS constant at pH 5.50)

Time (min)	pH	Temp °C	Residuals Copper (mg/l)
0	5.50	30.0	64.06
10		30.0	62.32
20		31.0	61.12
30		31.0	60.07
60		31.0	58.53
90		31.0	58.01
120		30.0	57.32
180		31.0	57.05

Table F7. Effect of pH increasing on Copper Removal (F-ICS without constant pH)

Time (min)	pH	Temp ⁰ C	Residuals Copper (mg/l)
0	5.50	30.0	64.06
10	5.85	30.0	60.06
20	5.89	30.0	56.78
30	5.94	30.0	54.46
60	6.12	30.0	52.07
90	6.08	30.0	50.82
120	6.26	30.0	49.16
180	6.45	30.0	47.98

Table F8. Effect of pH increasing on Copper Removal (T-ICS constant at pH 5.50)

Time (min)	pH	Temp ⁰ C	Residuals Copper (mg/l)
0	5.50	30.0	64.06
10		30.0	60.78
20		30.0	58.86
30		31.0	57.42
60		30.0	55.14
90		30.0	53.69
120		30.0	52.44
180		30.0	52.63

Table F9. Effect of pH increasing on Copper Removal (T-ICS without constant pH)

Time (min)	pH	Temp ⁰ C	Residuals Copper (mg/l)
0	5.50	32.0	64.06
10	5.71	32.0	59.96
20	5.77	32.0	57.24
30	5.81	32.0	55.44
60	5.95	32.0	51.87
90	5.98	32.0	50.43
120	6.01	32.0	49.14
180	6.11	32.0	48.16

Table F10. Adsorption Isotherm (1 g of F-ICS)

Time (min)	pH	Temp ⁰C	Residuals Copper (mg/l)
0	5.51	30.0	63.43
10	5.50	30.0	63.14
20	5.53	30.0	63.01
30	5.49	30.0	62.92
60	5.53	30.0	62.64
120	5.50	30.0	62.20
180	5.54	30.0	61.65
300	5.50	30.0	61.54

Table F11. Adsorption Isotherm (2 g of F-ICS)

Time (min)	pH	Temp ⁰C	Residuals Copper (mg/l)
0	5.51	29.8	63.50
10	5.53	30.0	62.63
20	5.53	30.0	62.03
30	5.51	30.2	61.51
60	5.54	30.2	61.09
120	5.55	30.3	60.28
180	5.54	30.1	59.94
300	5.55	30.5	59.67

Table F12. Adsorption Isotherm (4 g of F-ICS)

Time (min)	pH	Temp ⁰C	Residuals Copper (mg/l)
0	5.50	30.0	64.06
10	5.54	30.0	62.32
20	5.50	31.0	61.12
30	5.42	31.0	60.07
60	5.48	31.0	58.53
120	5.51	31.0	57.32
180	5.50	30.0	57.05
300	5.46	31.0	57.20

Table F13. Adsorption Isotherm (8 g of F-ICS)

Time (min)	pH	Temp °C	Residuals Copper (mg/l)
0	5.50	28.0	63.50
10	5.50	28.3	60.02
20	5.51	29.0	57.62
30	5.53	29.1	55.12
60	5.50	29.1	52.04
120	5.52	29.2	50.86
180	5.47	29.0	50.75
300	5.55	29.0	50.57

Table F14. Adsorption Isotherm (1 g of T-ICS)

Time (min)	pH	Temp °C	Residuals Copper (mg/l)
0	5.51	30.0	63.43
10	5.52	30.0	62.94
20	5.51	30.0	62.34
30	5.51	30.0	61.95
60	5.51	30.0	61.26
120	5.51	30.0	60.86
180	5.53	30.0	60.37
300	5.53	30.0	60.30

Table F15. Adsorption Isotherm (2 g of T-ICS)

Time (min)	pH	Temp °C	Residuals Copper (mg/l)
0	5.51	29.0	63.50
10	5.53	29.3	62.58
20	5.50	29.8	61.78
30	5.49	30.0	60.91
60	5.50	30.0	59.94
120	5.52	30.2	58.76
180	5.51	30.3	57.94
300	5.50	30.0	57.78

Table F16. Adsorption Isotherm (4 g of T-ICS)

Time (min)	pH	Temp °C	Residuals Copper (mg/l)
0	5.49	30.0	64.06
10	5.50	30.0	60.78
20	5.50	30.0	58.86
30	5.51	31.0	57.42
60	5.52	30.0	55.14
120	5.50	30.0	52.44
180	5.45	30.0	52.63
300	5.51	30.0	52.42

Table F17. Adsorption Isotherm (8 g of T-ICS)

Time (min)	pH	Temp °C	Residuals Copper (mg/l)
0	5.50	28.1	63.50
10	5.52	28.3	56.94
20	5.49	28.5	53.50
30	5.50	29.0	49.12
60	5.48	29.1	45.22
120	5.49	29.2	42.86
180	5.50	29.3	42.54
300	5.51	29.1	42.72

Table F18. Adsorption Isotherm (1 g of T-ICAO)

Time (min)	pH	Temp °C	Residuals Copper (mg/l)
0	5.50	32.2	64.20
10	5.48	32.6	63.72
20	5.50	32.3	63.53
30	5.55	32.5	63.38
60	5.51	33.3	63.05
120	5.51	33.8	62.55
180	5.50	34.2	62.45
300	5.53	34.2	62.34

Table F19. Adsorption Isotherm (2 g of T-ICAO)

Time (min)	pH	Temp ⁰C	Residuals Copper (mg/l)
0	5.50	32.2	64.20
10	5.50	32.8	63.83
20	5.51	32.3	63.16
30	5.53	32.5	62.74
60	5.50	33.3	61.93
120	5.55	33.8	60.92
180	5.51	34.2	60.71
300	5.54	34.3	60.83

Table F20. Adsorption Isotherm (4 g of T-IAO)

Time (min)	pH	Temp ⁰C	Residuals Copper (mg/l)
0	5.50	32.3	64.54
10	5.48	32.6	62.70
20	5.54	32.7	61.05
30	5.56	32.8	60.24
60	5.49	32.3	58.86
120	5.48	32.8	58.01
180	5.50	32.3	57.92
300	5.51	32.3	57.78

Table F21. Adsorption Isotherm (8 g of T-IAO)

Time (min)	pH	Temp ⁰C	Residuals Copper (mg/l)
0	5.52	33.3	64.48
10	5.50	33.3	61.17
20	5.55	33.5	59.11
30	5.56	33.7	55.94
60	5.50	33.2	52.98
120	5.59	33.2	52.59
180	5.54	33.6	52.38
300	5.59	33.9	52.35

Biography

Name: Mr. Setawat Homanee

Date of Birth: October 13, 1981

Place of Birth: Chonburi, Thailand

Nationality: Thai

Education:

2004 Bachelor Degree of Environmental Engineering,
Faculty of Engineering, King's Mongkut University of
Technology Thonburi, Bangkok, Thailand.



สถาบันวิทยบริการ
จุฬาลงกรณ์มหาวิทยาลัย